



# Improved simulation of the influence of the North Pacific Oscillation on El Niño-Southern Oscillation in CMIP6 than in CMIP5 models

Shangfeng Chen<sup>1,3</sup> · Wen Chen<sup>2</sup> · Renguang Wu<sup>4</sup> · Bin Yu<sup>5</sup> · Yuqiong Zheng<sup>2</sup> · Qingyu Cai<sup>2</sup> · Hasi Aru<sup>6</sup> · Xiaoqing Lan<sup>1</sup>

Received: 12 March 2024 / Accepted: 25 August 2024

© The Author(s), under exclusive licence to Springer-Verlag GmbH Germany, part of Springer Nature 2024

## Abstract

The North Pacific Oscillation (NPO) is an important intrinsic atmospheric pattern over the North Pacific. Observations have shown that the boreal winter NPO is a crucial precursor to the El Niño-Southern Oscillation (ENSO), with many ENSO events being preceded by the NPO. It is therefore imperative to assess the ability of current coupled climate models to reproduce the relationship between winter NPO and the subsequent winter ENSO. Previous studies have shown that most coupled climate models participating in the Coupled Model Intercomparison Project Phase 5 (CMIP5) underestimate the influence of winter NPO on the subsequent winter ENSO. Simulations from CMIP6, representing the latest generation of climate models, are now available. This study shows a remarkable improvement of the CMIP6 models in simulating the influence of winter NPO on the subsequent ENSO development compared to the CMIP5 models. This improvement is due to the improved air-sea interaction over the subtropical North Pacific in CMIP6. The enhanced air-sea interaction over the subtropical North Pacific promotes the equatorward propagation of the NPO-induced wind and SST anomalies, resulting in enhanced surface zonal wind anomalies over the tropical western Pacific, which further exert a stronger influence on the subsequent winter ENSO development by triggering the tropical Bjerknes positive air-sea interaction. The enhanced subtropical air-sea interaction is thought to be related to a southward shift of the North Pacific intertropical convergence zone in CMIP6 compared to CMIP5.

**Keywords** CMIP6 · CMIP5 · North Pacific Oscillation · El Niño-Southern Oscillation

## 1 Introduction

The El Niño and Southern Oscillation (ENSO) is the strongest air-sea coupled mode in the tropics, featured by large sea surface temperature (SST) anomalies in the tropical central-eastern Pacific and accompanied by oscillation in atmospheric mass between tropical western and eastern Pacific (Bjerknes 1969; Neelin et al. 1998; McPhaden et al. 2006; Alexander et al. 2002; Ren et al. 2020). Occurrences of ENSO events can exert substantial influences on climate, agriculture, water resources and ecosystems in distant areas through teleconnections (Wang et al. 2000; Alexander et al. 2002; Xie et al. 2009; Zhang et al. 2017, 2019; Yeh et al. 2018; Cai et al. 2020; Cai et al. 2024; and references therein). Additionally, ENSO serves as a vital source of sub-seasonal-to-seasonal climate predictability in many parts of the world, particularly in Asia, Africa and North America (Webster et al. 1998; Luo et al. 2008; Barnston et al. 2012; Chen et al. 2013; Tang et al. 2018; Wang 2019; Zhao et al.

✉ Wen Chen  
chenwen-dq@ynu.edu.cn

<sup>1</sup> Center for Monsoon System Research, Institute of Atmospheric Physics, Chinese Academy of Sciences, Beijing, China

<sup>2</sup> Department of Atmospheric Sciences, Yunnan University, Kunming 650500, China

<sup>3</sup> Key Laboratory of Meteorological Disaster, Ministry of Education & Collaborative Innovation Center on Forecast and Evaluation of Meteorological Disasters, Nanjing University of Information Science & Technology, Nanjing, China

<sup>4</sup> School of Earth Sciences, Zhejiang University, Hangzhou, China

<sup>5</sup> Climate Research Division, Environment and Climate Change Canada, Toronto, ON, Canada

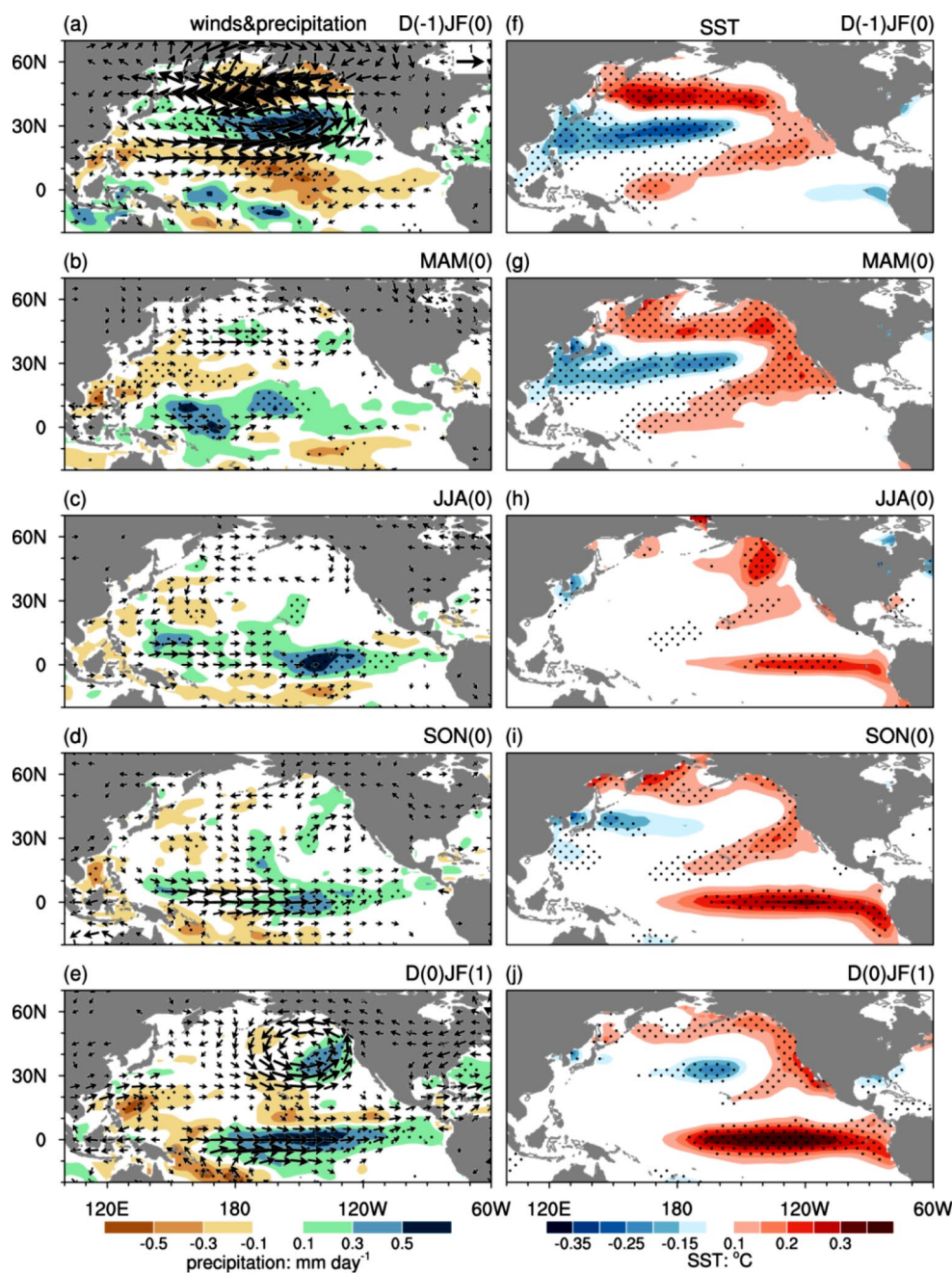
<sup>6</sup> Max Planck Institute for Meteorology, Bundesstrasse 53, 20146 Hamburg, Germany

2022). It is therefore critical to improve our understanding of ENSO variability.

In addition to the well-established tropical Pacific processes, recent studies have highlighted an important role of extratropical forcing in modulating the onset and evolution of ENSO (Vimont et al. 2001; Alexander et al. 2010; Chang et al. 2007; Nakamura et al. 2006; Yu and Kim 2011; Wang et al. 2011; Ham et al. 2013; Ding et al. 2015; Min et al. 2017; Amaya 2019; Chen et al. 2014, 2020a, 2023a, 2024a; Jia et al. 2021; Zheng et al. 2023, 2024). The North Pacific Oscillation (NPO), a dominant atmospheric variability over the North Pacific in boreal winter (Walker and Bliss 1932;

Rogers 1981; Song et al. 2021; Aru et al. 2022; Chen et al. 2024b), exerts a significant impact on the following winter ENSO via seasonal footprinting mechanism (Vimont et al. 2001, 2003; Alexander et al. 2010). Specifically, the positive phase of the winter NPO is related to a cyclonic anomaly over the subtropical North Pacific (Fig. 1a). The associated southwesterly wind anomalies contribute to subtropical warm SST anomalies by reducing total wind speed and upward latent heat flux (Figs. 1f-g). The subtropical warm SST anomalies maintain and extend southward into the tropical Pacific through the wind-evaporation-SST (WES) feedback, leading to low-level westerly wind

**Fig. 1** Anomalies of 850-hPa winds (vectors,  $\text{m s}^{-1}$ ) and precipitation (shadings,  $\text{mm day}^{-1}$ ) in (a) D(-1)JF(0), (b) MAM(0), (c) JJA(0), (d) SON(0), and (e) D(0)JF(1) regressed upon the D(-1)JF(0) NPO index during 1950–2020 in the observations. (f)–(j) are the same as in (a)–(e) but for SST anomalies. Stippling regions in (a)–(b) and (f)–(j) indicate precipitation and SST anomalies, respectively, significant at the 5% level



anomalies over the tropical western Pacific in spring and summer (Fig. 1c), which further lead to an El Niño-like anomaly pattern in the following winter via triggering oceanic Kelvin waves and the tropical Bjerknes positive air-sea interaction (Fig. 1c-e and h-j) (Bjerknes 1969; Vimont et al. 2003; Chen et al. 2014, 2023b; Alexander et al. 2010; Chen et al. 2015a; Cheng et al. 2023, 2024a). Apart from the seasonal footprinting mechanism described above, several recent studies argued that the winter NPO can also impact the subsequent ENSO via the trade wind charging mechanism (Anderson et al. 2013; Chakravorty et al. 2020) and the upper tropospheric process (Zhao et al. 2023a, b).

Many ENSO events (including the extremely strong El Niño events of 1982/83, 1997/98 and 2015/16, and the strong La Niña events of 1988/89, 1998/99, 1999/00 and 2007/08) were preceded by anomalous winter NPO years (Vimont et al. 2003; Chen and Wu 2018; Ding et al. 2022). The increased occurrence of central Pacific ENSO and multi-year El Niño events in recent decades has been linked to the winter NPO (Yu and Kim 2011; Yeh et al. 2015; Ding et al. 2022). Furthermore, Chen et al. (2024) suggested that the impact of the winter NPO on the following winter ENSO would be significantly strengthened in a warming climate. Given the pivotal role of NPO on ENSO, it is of utmost importance to evaluate the representation of the winter NPO-ENSO connection in the current climate models. Studies indicated that many climate models participating in CMIP5 cannot simulate the impact of winter NPO on ENSO, which is due to the weak WES feedback in the subtropical North Pacific (Wang et al. 2019; Park et al. 2021). Model simulations from the CMIP6 (Eyring et al. 2016; Chen et al. 2021) are now available, and an important priority is therefore to evaluate the representation of the winter NPO-ENSO connection in CMIP6 and compare against that in CMIP5 (Taylor et al. 2012). Our present study aims to answer the following questions: (1) How well do the CMIP6 models reproduce the influence of the winter NPO on ENSO? (2) Does CMIP6 represent better the winter NPO-ENSO relationship than CMIP5? and (3) if so, what are the factors that lead to the improvement. The answers to these questions have important implications for the further improvement of ENSO prediction in current climate models. In the present study, we show that CMIP6 models have a notable improvement in simulating the impact of winter NPO on the subsequent winter ENSO. The factor leading to the improvement is further examined.

The structure of this study is organized as follows. Section 2 describes the data and method employed in this study. Section 3 examines the performances of the coupled climate models in CMIP5 and CMIP6 in simulating the influence of the winter NPO on the following winter ENSO. We show that the CMIP6 has an improvement in reproducing the

observed impact of the winter NPO on the following winter ENSO. Section 4 examines the factors responsible for the improvement. Section 5 provides a summary.

## 2 Data and method

We use outputs from historical simulation of 37 CMIP5 models (Taylor et al. 2012) and 39 CMIP6 models (Eyring et al. 2016). Variables used include monthly mean sea level pressure (SLP), winds, precipitation, surface wind stress, and surface temperature. Outputs of historical simulation from the first available ensemble member of CMIP5 and CMIP6 models were used. Information of the CMIP6 and CMIP5 used in this study is provided in Tables 1 and 2, respectively. We compare CMIP5 and CMIP6 results over the period 1900–2003. This study also uses monthly atmospheric data from the NCEP-NCAR reanalysis over the period 1948–2022 (Kalnay et al. 1996). Monthly SST data were obtained from the ERSSTv5 (Huang et al. 2017). Monthly precipitation data were derived from the Global Precipitation Climatology Project (GPCP) (Adler et al. 2003). For the sake of description, data from the NCEP-NCAR, ERSSTv5 and GPCP are referred to as “observations”.

All data are detrended before the analysis. In addition, all variables from the observations, CMIP5 and CMIP6 are converted to a common horizontal resolution of  $2^\circ \times 2^\circ$  to facilitate comparison and to calculate the multi-model ensemble mean (MME). The Niño3.4 SST index, defined as area-averaged SST anomalies in the region of  $5^\circ\text{S}$ – $5^\circ\text{N}$  and  $120^\circ$ – $170^\circ\text{W}$ , is used to represent ENSO variability. The NPO pattern is represented by the second EOF (EOF2) of the observed SLP anomalies over the North Pacific ( $20^\circ$ – $70^\circ\text{N}$ ,  $120^\circ\text{E}$ – $120^\circ\text{W}$ ) (Linkin and Nigam 2008; Yu and Kim 2011). The observed NPO index is calculated by projecting the NCEP-NCAR SLP anomalies onto the EOF2. The NPO indices in the CMIP5 and CMIP6 models are obtained by projecting the simulated SLP anomalies onto the observed EOF2 of SLP anomalies as in Lee et al. (2019), Aru et al. (2021) and Chen et al. (2021). Following previous studies (Vimont et al. 2003; Alexander et al. 2010), the winter ENSO signal has been linearly removed from the concurrent winter NPO index prior to the analysis. This ensures that the effect of winter NPO on the subsequent winter ENSO is independent of the ENSO cycle (Vimont et al. 2003; Alexander et al. 2010).

We employ a bootstrap test technique to estimate whether difference of two quantities between the CMIP5 and CMIP6 ensemble mean is statistically significant (Austin and Tu 2004). Take the correlation coefficient between  $D(-1)\text{JF}(0)$  NPO index and  $D(0)\text{JF}(1)$  Niño3.4 index as an example. Here, (-1), (0) and (1) denote the previous, current

**Table 1** Information of 39 CMIP6 models employed in this study

Abbr. Name	Institute	Country	Ensemble
ACCESS-CM2	CSIRO	Australia	rlilp1f1
ACCESS-ESM1-5	CSIRO	Australia	rlilp1f1
AWI-CM-1-1-MR	AWI	Germany	rlilp1f1
BCC-CSM2-MR	BCC	China	rlilp1f1
CanESM5	CCCma	Canada	rlilp1f1
CanESM5-CanOE	CCCma	Canada	rlilp2f1
CAMS-CSM1-0	CAMS	China	rlilp1f1
CAS-ESM2-0	CAS	China	rlilp1f1
CESM2	NCAR	USA	rlilp1f1
CESM2-WACCM	NCAR	USA	rlilp1f1
CIESM	Tsinghua University	China	rlilp1f1
CMCC-CM2-SR5	CMCC	Italy	rlilp1f1
CMCC-ESM2	CMCC	Italy	rlilp1f1
CNRM-CM6-1	CNRM	France	rlilp1f2
CNRM-ESM2-1	CNRM	France	rlilp1f2
E3SM-1-1	DOE	USA	rlilp1f1
EC-Earth3	Europe consortium	Europe consortium	rlilp1f1
EC-Earth3-Veg	Europe consortium	Europe consortium	rlilp1f1
EC-Earth3-Veg-LR	Europe consortium	Europe consortium	rlilp1f1
FGOALS-f3-L	CAS	China	rlilp1f1
FGOALS-g3	CAS	China	rlilp1f1
FIO-ESM-2-0	FIO	China	rlilp1f1
GFDL-CM4	NOAA, GFDL	USA	rlilp1f1
GFDL-ESM4	NOAA, GFDL	USA	rlilp1f1
HadGEM3-GC31-LL	MOHC	UK	rlilp1f3
IITM-ESM	CCCR-IITM	India	rlilp1f1
INM-CM5-0	INM	Russia	rlilp1f1
IPSL-CM6A-LR	IPSL	France	rlilp1f1
KACE-1-0-G	NIMS-KMA	Korea	rlilp1f1
MIROC-ES2L	JAMSTEC	Japan	rlilp1f2
MIROC6	JAMSTEC	Japan	rlilp1f1
MPI-ESM1-2-HR	MPI-M	Germany	rlilp1f1
MPI-ESM1-2-LR	MPI-M	Germany	rlilp1f1
MRI-ESM2-0	MRI	Japan	rlilp1f1
NESM3	NUIST	China	rlilp1f1
NorESM2-MM	NCC	Norway	rlilp1f1
NorESM2-LM	NCC	Norway	rlilp1f1
TaiESM1	AS-RCEC	Chinese Taipei	rlilp1f1
UKESM1-0-LL	MOHC	UK	rlilp1f2

and subsequent years, respectively. First, we calculate the correlation coefficient between the  $D(-1)JF(0)$  NPO index and  $D(0)JF(1)$  Niño3.4 index over the period 1900–2003 in 37 CMIP5 and 39 CMIP6 models, respectively. Second, the correlation coefficients calculated in the 37 CMIP5 and 39 CMIP6 models are resampled randomly to construct respective 10,000 realizations. In this random resampling process, the correlation coefficient in any models can be chosen again. Third, the standard deviations of the 10,000

**Table 2** Information of 37 CMIP5 models employed in this study

Abbr. Name	Institute	Country	Ensemble
ACCESS1-0	CSIRO	Australia	rlilp1
ACCESS1-3	CSIRO	Australia	rlilp1
bcc-csm1-1	BCC	China	rlilp1
bcc-csm1-1-m	BCC	China	rlilp1
CanESM2	CCCma	Canada	rlilp1
CCSM4	NCAR	USA	rlilp1
CESM1-BGC	NCAR	USA	rlilp1
CESM1-CAM5	NCAR	USA	rlilp1
CESM1-FASTCHEM	NCAR	USA	rlilp1
CMCC-CM	CMCC	Italy	rlilp1
CMCC-CMS	CMCC	Italy	rlilp1
CNRM-CM5	CNRM	France	rlilp1
CSIRO-Mk3-6-0	CSIRO-QCCCE	Australia	rlilp1
FGOALS-g2	LASG	China	rlilp1
FGOALS-s2	LASG	China	rlilp1
FIO-ESM	FIO	China	rlilp1
GFDL-CM3	NOAA	USA	rlilp1
GFDL-ESM2G	NOAA	USA	rlilp1
GISS-E2-H	NASA	USA	rlilp1
GISS-E2-H-CC	NASA	USA	rlilp1
GISS-E2-R	NASA	USA	rlilp1
GISS-E2-R-CC	NASA	USA	rlilp1
HadCM3	MOHC	UK	rlilp1
HadGEM2-AO	MOHC	UK	rlilp1
inmcm4	INM	Russia	rlilp1
IPSL-CM5A-LR	IPSL	France	rlilp1
IPSL-CM5A-MR	IPSL	France	rlilp1
IPSL-CM5B-LR	IPSL	France	rlilp1
MIROC-ESM	MIROC	Japan	rlilp1
MIROC-ESM-CHEM	MIROC	Japan	rlilp1
MIROC5	MIROC	Japan	rlilp1
MPI-ESM-LR	MPI	Germany	rlilp1
MPI-ESM-MR	MPI	Germany	rlilp1
MPI-ESM-P <sup>rr</sup>	MPI	Germany	rlilp1
MRI-CGCM3	MRI	Japan	rlilp1
NorESM1-M	NCC	Norway	rlilp1
NorESM1-ME	NCC	Norway	rlilp1

inter-realizations of the correlation coefficients in the CMIP5 and CMIP6 models are calculated, respectively. Then, if the sum of the standard deviations of the two 10,000 realizations is smaller than the difference of correlation coefficient between the CMIP5 MME and CMIP6 MME, then the difference is considered as significant. Similar processes were applied to estimate whether differences in the other quantities between CMIP5 and CMIP6 are significant, for example, MAMJJA(0) 850 hPa zonal wind anomalies in the tropical western Pacific, MAMJJA(0) precipitation anomalies in the subtropical North Pacific and  $D(0)JF(1)$  SST anomalies in the tropical central-eastern Pacific regressed upon the  $D(-1)JF(0)$  NPO index.

### 3 Improved NPO-ENSO connection in CMIP6

To investigate the relationship between the winter NPO and ENSO, we first assess the performances of the CMIP5 and CMIP6 models in capturing the NPO pattern. The spatial pattern of the winter NPO is described by the D(-1)JF(0) SLP anomalies regressed on the normalized D(-1)JF(0) NPO index. In this study, positive phase of winter NPO is

characterized by positive SLP anomalies over mid-latitudes and negative SLP anomalies over subtropics. MMEs of the CMIP5 and CMIP6 models simulate well the spatial pattern of NPO featured by a meridional SLP dipole anomaly over the North Pacific (Fig. 2a-c). The pattern correlations between observed and simulated SLP anomalies in CMIP5/CMIP6 models over the North Pacific are greater than 0.8 (Fig. 2d-e). ENSO has a winter phase locking feature in the

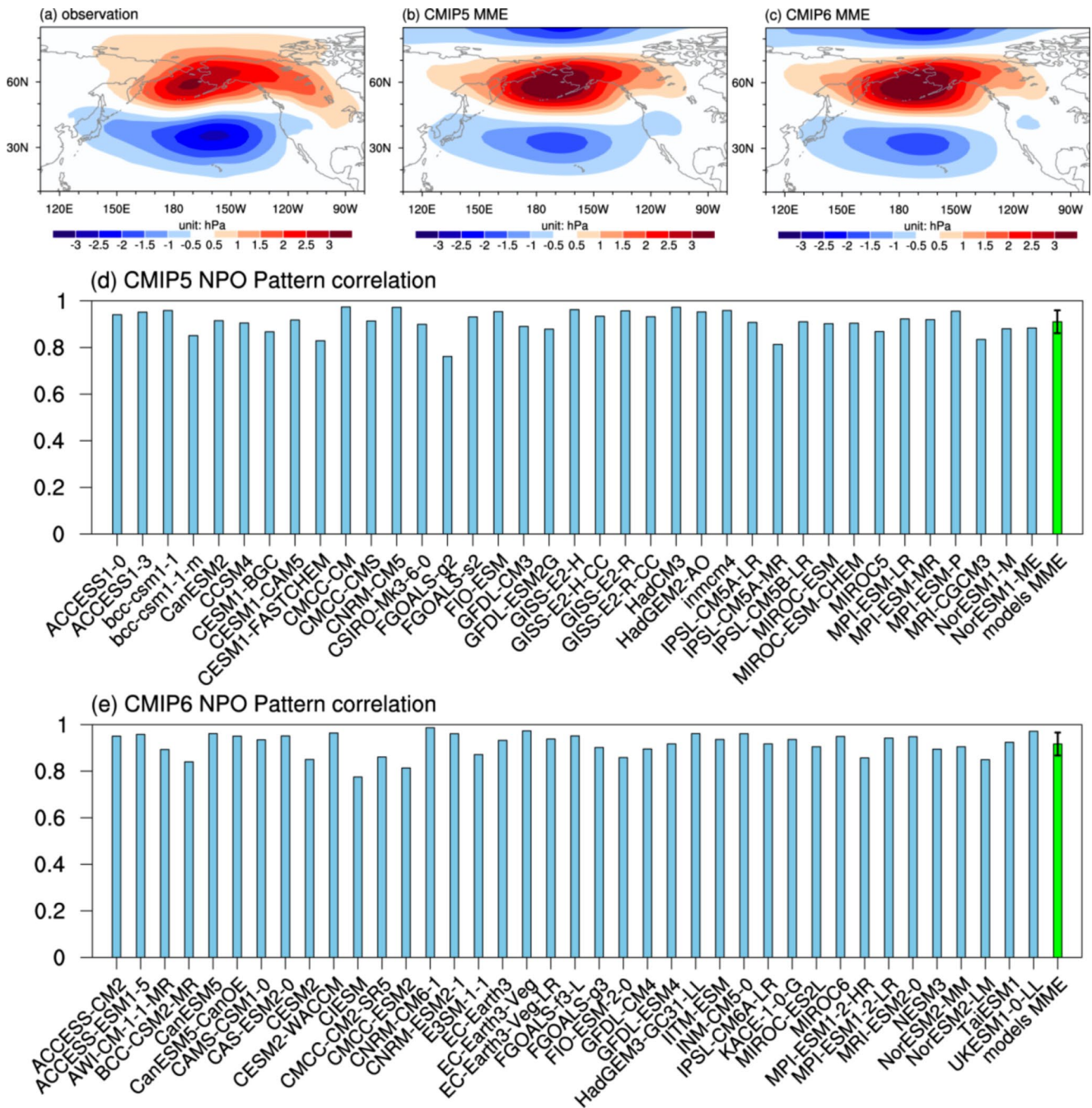


**Fig. 2** SLP anomalies in D(-1)JF(0) regressed upon the D(-1)JF(0) NPO index in (a) the observations, (b) the MME of the 37 CMIP5 models, and (c) the MME of the 39 CMIP6 models. (d) Pattern correlations of D(-1)JF(0) NPO-related D(-1)JF(0) SLP anomalies over

North Pacific (20°-70°N, 120°E-100°W) between observations and 37 CMIP5 models. Green bar indicates MME of the CMIP5 models, with error bar representing one standard deviation among the models. (e) is the same as (d), but for the CMIP6 models

observations (Wang et al. 2000; Zhang et al. 2017; Yeh et al. 2018). Most models in CMIP5 and CMIP6 have a good ability to simulate the seasonality of the ENSO, with the maximum standard deviation of the Niño3.4 SST occurring in the boreal winter. From the MME perspective, it shows that the CMIP6 has an improvement in simulating the seasonality of the ENSO, with a larger amplitude of the Niño3.4 SST index in boreal winter in CMIP6 compared to CMIP5 (Fig. 3).

Next, we examine the performance of the CMIP models in simulating the relationship between winter NPO and following winter ENSO. Figure 4a and b show the correlation coefficients between the D(-1)JF(0) NPO index and the D(0)JF(1) Niño3.4 index in observations as well as in 37 CMIP5 and 39 CMIP6 models during 1900–2003. In CMIP5, approximately 46% (17 out of 37 models) produce a

significant positive NPO-ENSO relationship (light blue bars in Fig. 4a). This proportion is consistent with that reported in Park et al. (2021). The MME of the correlations is 0.14, considerably lower than the observed ( $r=0.31$ ) (Fig. 4a). In contrast, a higher proportion of CMIP6 models (74%, 29 out of 39 models; light blue bars in Fig. 4b) produce a significant positive correlation between the D(-1)JF(0) NPO index and the D(0)JF(1) Niño3.4 index. The MME correlation in the 39 CMIP6 models ( $r=0.22$ ) is closer to the observation (Fig. 4b). The NPO-ENSO correlation in CMIP6 MME is 57% larger than that in the CMIP5 (Fig. 4a and b). Importantly, the increase in the NPO-ENSO correlation from the CMIP5 to the CMIP6 based on the MME is statistically significant at the 95% confidence level based on a bootstrap test. This suggests that the CMIP6 models exhibit an improved capability to simulate the connection between the winter NPO and the subsequent ENSO.

Previous studies have shown that the influence of the boreal winter NPO on the subsequent ENSO is unstable, showing significant interdecadal changes in the past (Chen et al. 2019; Park et al. 2021). Therefore, one might wonder whether the results obtained are sensitive to the period of analysis. To address this issue, we have examined the correlation coefficients between the winter NPO index and the following winter Niño3.4 index over different periods (e.g. over 1948–2003, Fig. 4c-d) in CMIP5 and CMIP6 models. The results are found to be insensitive to the choice of analysis periods (Fig. 4).

The above analysis suggests that the CMIP6 models have improved the simulation of the impact of the winter NPO on ENSO. One might want to know which models have improved this relationship. It should be noted that not all models participated in both CMIP5 and CMIP6 (Tables 1 and 2). In addition, some institutes have different versions of models (e.g. IPSL, MIROC, MPI, etc.). When the models come from the same institute, we consider their ensemble mean. Figure 5 shows the correlation coefficient between the D(-1)JF0 NPO index and the D(0)JF(1) Niño3.4 index over the period 1900–2003 for the models from 16 institutes that participated in both CMIP5 and CMIP6. It shows that models from 11 of the 16 institutes (about 69%) have improved the simulation of the relationship between the winter NPO and the following winter ENSO.

The improvement of the CMIP6 models in producing the impact of winter NPO on ENSO is further supported by comparing the seasonal evolution of SST and 850-hPa wind anomalies through regression analysis on the NPO. In the CMIP6 MME, a positive winter NPO is associated with a north-south dipole pattern in atmospheric circulation over the North Pacific. This pattern consists of an anomalous anticyclone over mid-latitudes and an anomalous cyclone over the subtropics (Fig. 6a). The associated southwesterly

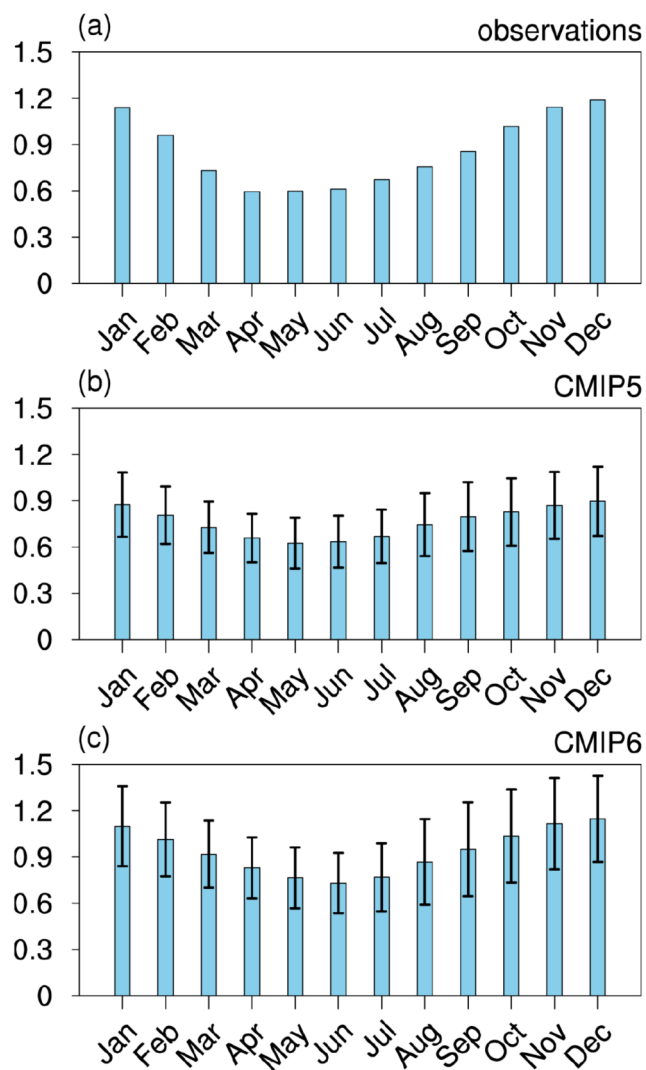
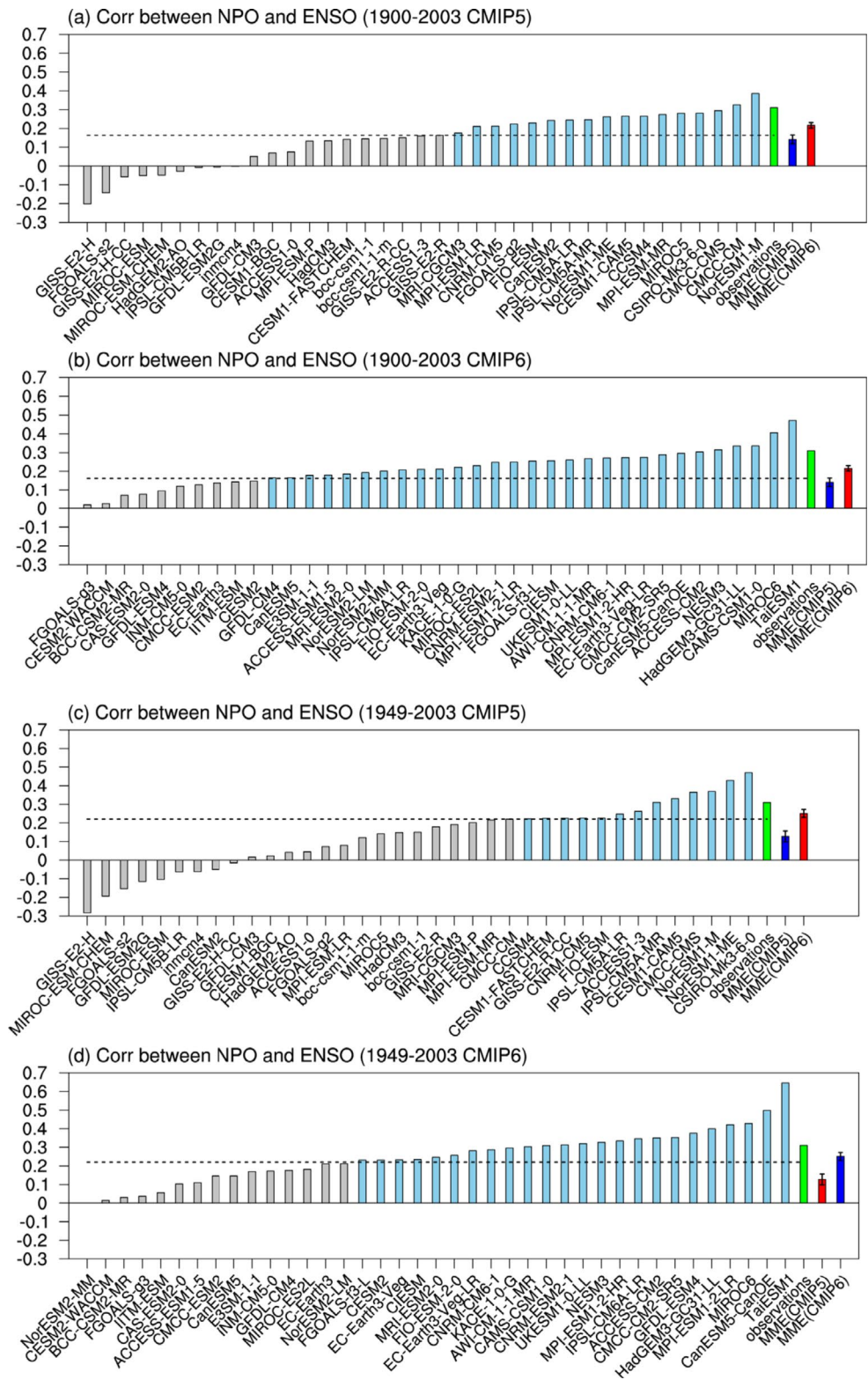


**Fig. 3** Standard deviation ( $^{\circ}\text{C}$ ) of the monthly Niño3.4 index in the (a) observations, and MME of the (b) 37 CMIP5 and 39 CMIP6 models. Error bars in (b) and (c) represent one standard deviation among the models

**Fig. 4** Correlation between D(-1) JF0 NPO index and D(0)JF(1) Niño3.4 index during 1900–2003 in (a) 37 CMIP5 and (b) 39 CMIP6 models. Horizontal line in (a)–(b) indicates the correlation significant at the 5% level. Green bar indicates the observed result. Blue (red) bar indicates the CMIP5 (CMIP6) MME, error bars denoting one standard deviation (s.d.) of the 10,000 resampling with replacement of the bootstrap test. (c)–(d) are the same as (a)–(b), but during 1948–2003



wind anomalies over the subtropical North Pacific oppose the prevailing northeasterly winds, leading to a decrease in total wind speed and a reduction in upward surface latent heat flux (Vimont et al. 2001, 2003). The decrease in surface

heat flux from the ocean to the atmosphere contributes to SST warming in the subtropical North Pacific (SNP) in the following spring (Fig. 6b). The SST warming in the subtropical North Pacific persists and extends southward into

**Fig. 5** Correlation between the D(-1)JF0 NPO index and the D(0)JF(1) Niño3.4 index during 1900–2003 for the models participated in CMIP5 and CMIP6 from 16 institutes. Blue (red) bar indicates the CMIP5 (CMIP6), error bars in the MME denoting one standard deviation (s.d.) of the 10,000 resampling with replacement of the bootstrap test

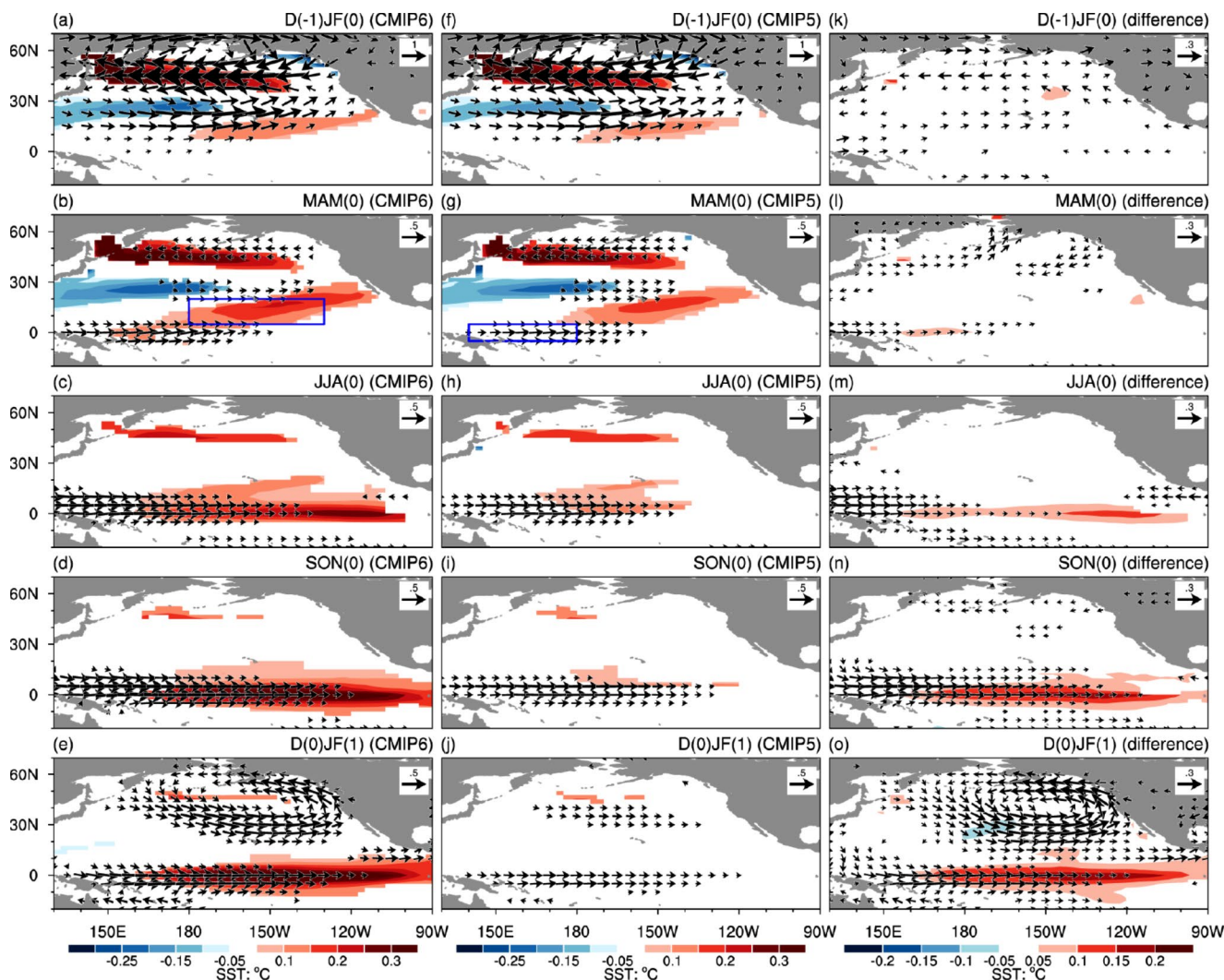
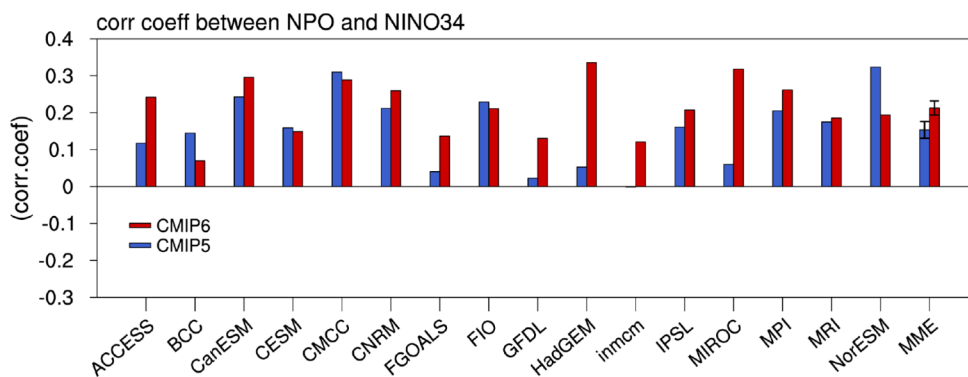


**Fig. 6** Anomalies of SST and 850-hPa winds in D(-1)JF(0), MAM(0), JJA(0), SON(0), and D(0)JF(1) regressed upon the D(-1)JF(0) NPO index over 1900–2003 for the CMIP6 MME (left), and CMIP5 MME

(middle), and the differences between CMIP6 and CMIP5 (right). Only SST anomalies significant at the 5% level are shown

the tropical Pacific through the WES feedback mechanism (Xie and Philander 1994; Vimont et al. 2001, 2003). This leads to low-level westerly wind anomalies over the tropical western Pacific in the following summer via a Rossby

wave-type atmospheric response (Fig. 6c). The low-level westerly wind anomalies over the tropical western Pacific further contribute to the formation of an El Niño warming pattern in the subsequent winter by triggering a tropical



Bjerknes feedback (Fig. 6d-e; Bjerknes 1979; Vimont et al. 2001, 2003).

In the CMIP5 MME, a meridional dipole pattern of atmospheric anomalies is observed over the North Pacific in winter, with a similar amplitude compared to the CMIP6 (Fig. 6f). In addition, a tripolar pattern of SST anomaly appears in the North Pacific, characterized by warm anomalies in the subtropical North Pacific and mid-latitudes and cold anomalies in the western North Pacific around 20°-30°N (Fig. 6g). However, the D(-1)JF(0) NPO-induced low-level westerly wind anomalies over the tropical western Pacific are much weaker in the CMIP5 compared to the CMIP6 ensemble mean (Fig. 6h). Consequently, the response of SST anomalies in the tropical central and eastern Pacific (TCEP) in the following winter is also weaker in CMIP5 (Fig. 6i-j). In particular, D(0)JF(1) SST anomalies averaged in the tropical central-eastern Pacific (TCEP, 5°S-5°N, 180°-90°W) in response to the D(-1)JF(0) NPO in the CMIP5 MME is 0.13°C, which is 85% weaker than the corresponding response (0.24°C) in the CMIP6 (Fig. 7a). The difference in the response of the D(0)JF(1) SST anomalies in the TCEP between the CMIP5 and CMIP6 is significant according to the bootstrap test (Fig. 7a). We have also compared the difference in the D(0)JF(1) precipitation response. The D(0)JF(1) TCEP precipitation response is significantly larger in the CMIP6 (0.40 mm day<sup>-1</sup>) compared to that in the CMIP5 (0.21 mm day<sup>-1</sup>) (Fig. 7b). The above results

indicate that CMIP6 models have an improvement in simulating the impact of the winter NPO on the following winter ENSO compared to CMIP5 models.

#### 4 Factors for the improved NPO-ENSO connection in CMIP6

The mechanisms underlying the improved performance of CMIP6 models in reproducing the NPO-ENSO connection are further explored. Previous studies have indicated the importance of the southern lobe of the winter NPO in the seasonal footprinting mechanism for ENSO development (Vimont et al. 2003; Park et al. 2021; Chen and Yu 2020). However, the differences in the D(-1)JF(0) 850-hPa wind anomalies over the North Pacific related to the D(-1)JF(0) NPO between the CMIP5 and CMIP6 MMEs are weak. In addition, there is little correlation between the inter-model difference in the intensity of the southern lobe of the NPO and the D(0)JF(1) SST TCEP responses in both the CMIP5 and CMIP6 models (Fig. 8). This suggests that the enhanced impact of the winter NPO on the following winter ENSO in CMIP6 is unlikely due to the divergence of the NPO characteristics.

Winter NPO-related low-level winds and SST anomalies extend southward into the tropical western-central Pacific in the following spring and summer through the WES feedback mechanism (Vimont et al. 2001; Alexander et al. 2010). These low-level zonal wind anomalies in the tropical western-central Pacific trigger oceanic Kelvin waves and the positive Bjerknes air-sea feedback, which further contribute to the development of ENSO in the following autumn and winter (Vimont et al. 2001; Chen et al. 2020a, b; Alexander et al. 2010). Studies have indicated that a CMIP5 model's ability to simulate the NPO-ENSO connection is closely related to the strength of the WES feedback in the subtropical North Pacific (Wang et al. 2019; Park et al. 2021). In particular, many CMIP5 models tend to underestimate the strength of the response of precipitation and atmospheric anomalies to the NPO-generated subtropical SST anomalies in the spring and summer (Wang et al. 2019; Park et al. 2021), leading to a weak influence of the NPO on ENSO.

To compare the strength of air-sea coupling in the subtropical North Pacific between CMIP5 and CMIP6, we follow the method used in previous studies (Wang et al. 2019; Park et al. 2021; Zheng et al. 2021). First, we define a subtropical North Pacific (SNP) SST index using area-mean SST anomalies averaged in the region of 5°-20°N and 140°E-120°W in MAMJJA(0). Then, we regress the precipitation anomalies in MAMJJA(0) onto the normalized SNP SST index for each CMIP5/CMIP6 model. The amplitude of precipitation anomalies in MAMJJA(0) averaged over

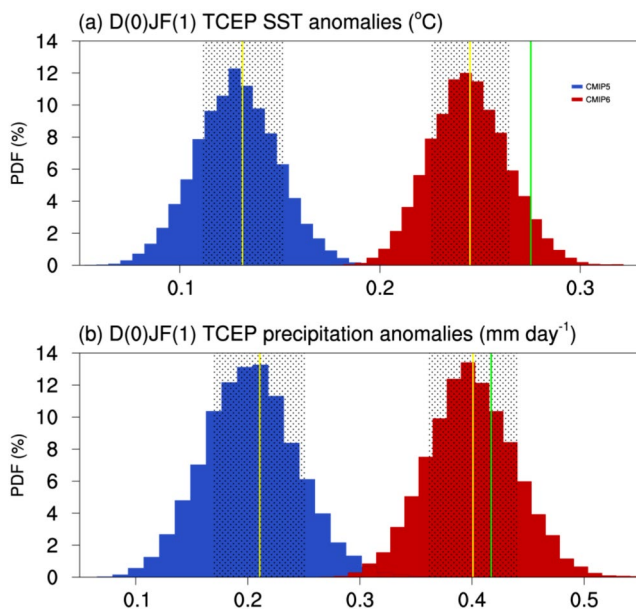
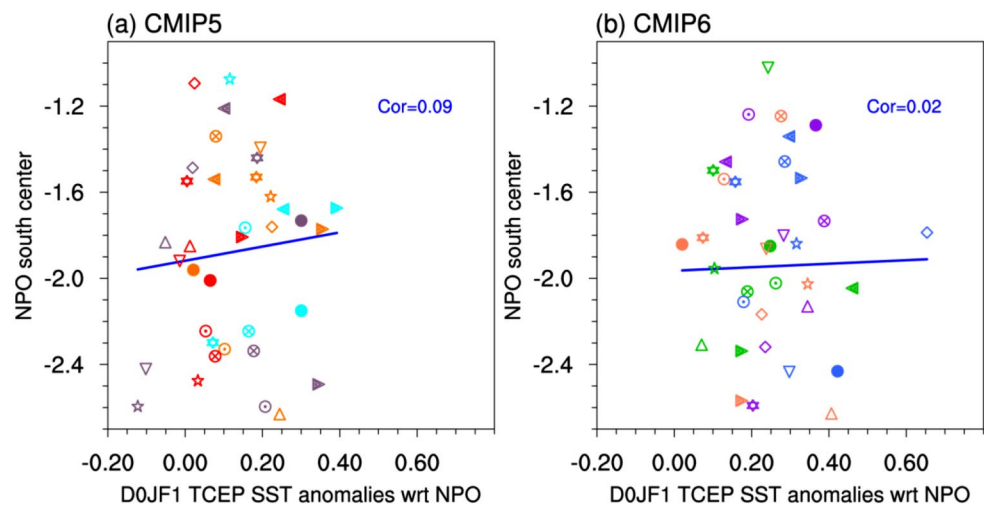


**Fig. 7** Probability distributions of the 10,000 resampling with replacement of the bootstrap test for the D(0)JF(1) (a) SST and (b) precipitation anomalies in the tropical central-eastern Pacific (TCEP) obtained by regression on the D(-1)JF(0) NPO index for the CMIP5 (blue) and CMIP6 (red). Yellow lines in (a)-(b) indicate the mean value of the 10,000 resampling, with stippling regions indicating one s.d. of the 10,000 resampling. Green line indicates the observed result

**Fig. 8** Scatter plot of D(0)JF(1) TCEP SST anomalies regressed upon the D(-1)JF(0) NPO versus intensity of the southern center of the NPO among the (a) 37 CMIP5 and (b) 39 CMIP6 models. Intensity of the southern center of the NPO is defined as the minimum value of the D(-1)JF(0) SLP anomalies regressed upon the D(-1)JF(0) NPO index over the subtropical Northern Pacific



the subtropical North Pacific serves as an indicator of the intensity of the WES feedback (Wang et al. 2019; Park et al. 2021; Zheng et al. 2021).

From an inter-model perspective, a model with a stronger subtropical North Pacific WES feedback corresponds to stronger NPO-generated precipitation anomalies over the subtropical Pacific (Fig. 9a-b). This would induce stronger low-level zonal wind anomalies over the tropical western Pacific (Fig. 9d-e) and exert a stronger influence on the subsequent winter ENSO (Fig. 9g-h). The inter-model relationship between the strength of subtropical WES feedback in MAMJJA0, the NPO-generated low-level zonal wind anomalies in MAMJJA0, and the NPO-generated SST anomalies in the tropical central-eastern Pacific in D(0)JF(1) are significant at the 99% confidence level for both the CMIP5 and CMIP6 models (Fig. 9a-b, c-d and e-f). From the MME perspective, it is clear that the WES feedback strength in the subtropical North Pacific is significantly stronger in CMIP6 than in CMIP5 (Fig. 10a). The enhanced subtropical WES feedback in CMIP6 (Fig. 10a) corresponds to enhanced NPO-generated subtropical North Pacific precipitation anomalies (Fig. 10b) and strengthened low-level zonal wind anomalies over the tropical western Pacific (Fig. 10c), which further contribute to a stronger impact of the winter NPO on the following winter ENSO. Therefore, the improved simulation of the winter NPO-ENSO connection in CMIP6 models can be attributed to the enhanced subtropical WES feedback, which was underestimated by CMIP5 models as reported in previous studies (Wang et al. 2018; Park et al. 2021).

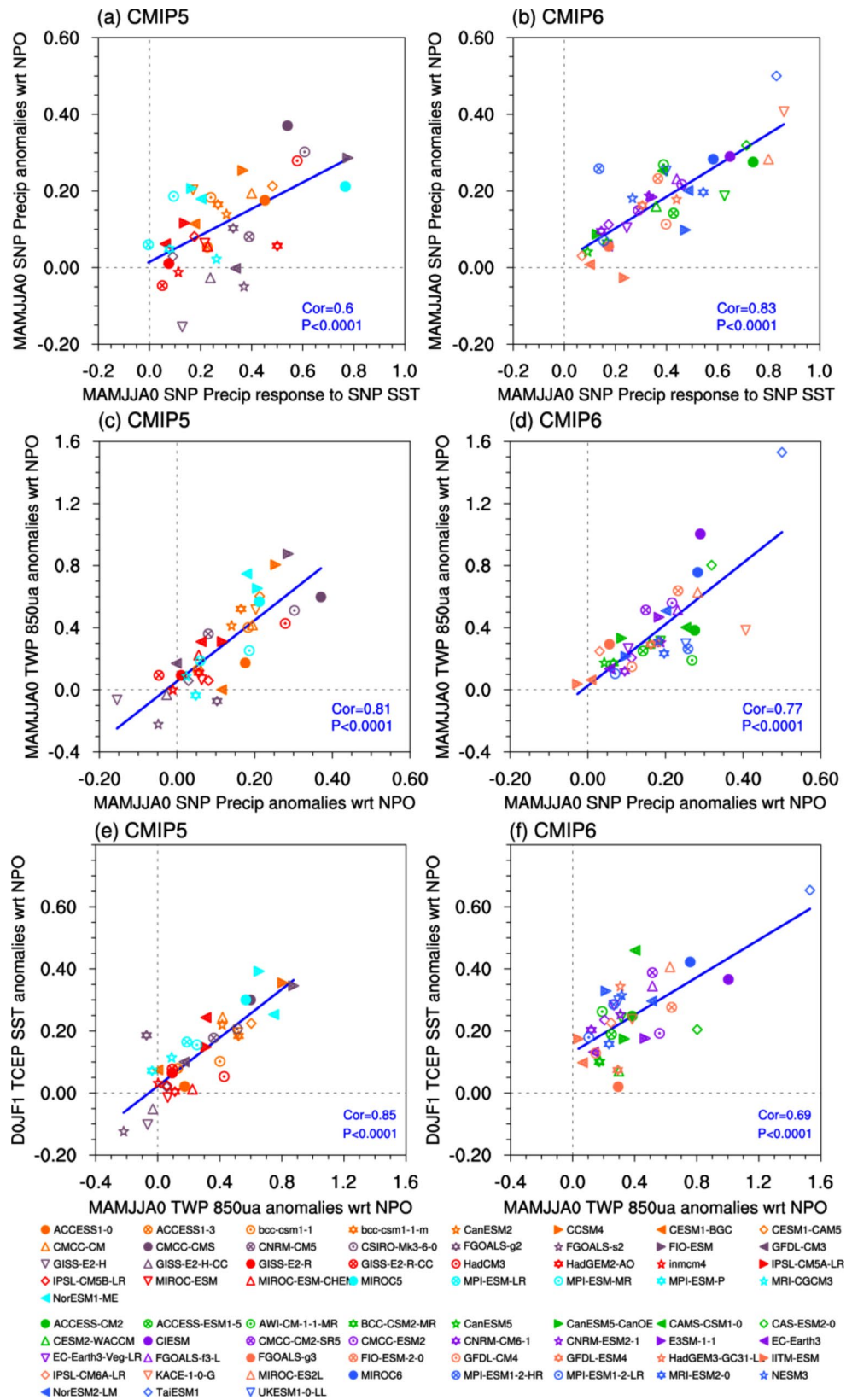
We then investigated the factors for the enhanced WES feedback in CMIP6. Studies have shown that the subtropical WES feedback strength related to the seasonal footprinting mechanism was remarkably modulated by the mean states, including the strength of the mean northeasterly trade winds and the meridional position of the North Pacific ITCZ

(Vimont et al. 2008; Vimont 2010; Zhang et al. 2014; Amaya 2019; Zheng et al. 2021, 2023). In terms of the role of the mean trade winds, the subtropical WES efficiency would be higher (lower) if climatological trade winds were stronger (weaker) (Vimont et al. 2008; Vimont 2010; Amaya 2019; Zheng et al. 2023). Enhancement of the mean trade winds could increase the sensitivity of surface evaporation to unit change of surface winds, and vice versa (Vimont et al. 2009; Vimont 2010; Amaya 2019). However, there is no evidence to support that the enhanced subtropical WES feedback in CMIP6 is due to the strengthened mean trade winds (figure not shown).

In terms of the role of mean ITCZ, previous studies have suggested that the equatorward propagation of the NPO-generated subtropical surface winds and SST anomalies to the tropical Pacific is closely related to the meridional shift of mean ITCZ (Okajima et al. 2003; Xiang et al. 2013; Zhang et al. 2014; Zheng et al. 2023). If mean ITCZ moves southward, the NPO-related surface winds and SST anomalies can more effectively extend into the deep tropics through the WES feedback (Okajima et al. 2003; Xiang et al. 2013; Zhang et al. 2014; Zheng et al. 2023). This is because the background southwesterly winds to the south of the ITCZ can suppress the WES feedback process (Okajima et al. 2003; Zhang et al. 2014; Zheng et al. 2023).

To confirm the above finding, we examined the inter-model relationship between the latitude of the Pacific ITCZ in spring-summer and the subtropical WES strength. Here, the ITCZ latitude is calculated by averaging the latitudes where the spring-summer-mean precipitation reaches a maximum over the region of 160°E-130°W. Figure 11a-b shows the scatter plot of the meridional location of the MAMJJA0-mean Pacific ITCZ versus the subtropical WES feedback strength among the CMIP5 and CMIP6 models. The correlation coefficients between the two variables in Fig. 11a-b for CMIP5 and CMIP6 are  $-0.38$  and  $-0.52$ ,

**Fig. 9** Scatter plot of MAMJJA(0) precipitation anomalies in the subtropical North Pacific (SNP, box in Fig. 6b) regressed upon the MAMJJA(0) SNP SST index (X-axis,  $\text{mm day}^{-1}$ ) versus MAMJJA(0) SNP precipitation anomalies regressed upon the D(-1)JF(0) NPO index (Y-axis,  $\text{mm day}^{-1}$ ) among the (a) 37 CMIP5 and (b) 39 CMIP6 models. (c)-(d) as in (a)-(b), but for scatter plot of MAMJJA(0) SNP precipitation anomalies regressed upon the D(-1)JF(0) NPO index (X-axis,  $\text{mm day}^{-1}$ ) versus MAMJJA(0) 850-hPa zonal wind anomalies in the tropical western Pacific (TWP, box in Fig. 6g) regressed upon the D(-1)JF(0) NPO index (Y-axis,  $\text{m s}^{-1}$ ). (e)-(f) as in (a)-(b), but for scatter plot of MAMJJA(0) TWP 850-hPa zonal wind anomalies regressed upon the D(-1)JF(0) NPO index (X-axis,  $\text{m s}^{-1}$ ) versus D(0)JF(1) TCEP SST anomalies regressed upon the D(-1)JF(0) NPO index (Y-axis,  $^{\circ}\text{C}$ )



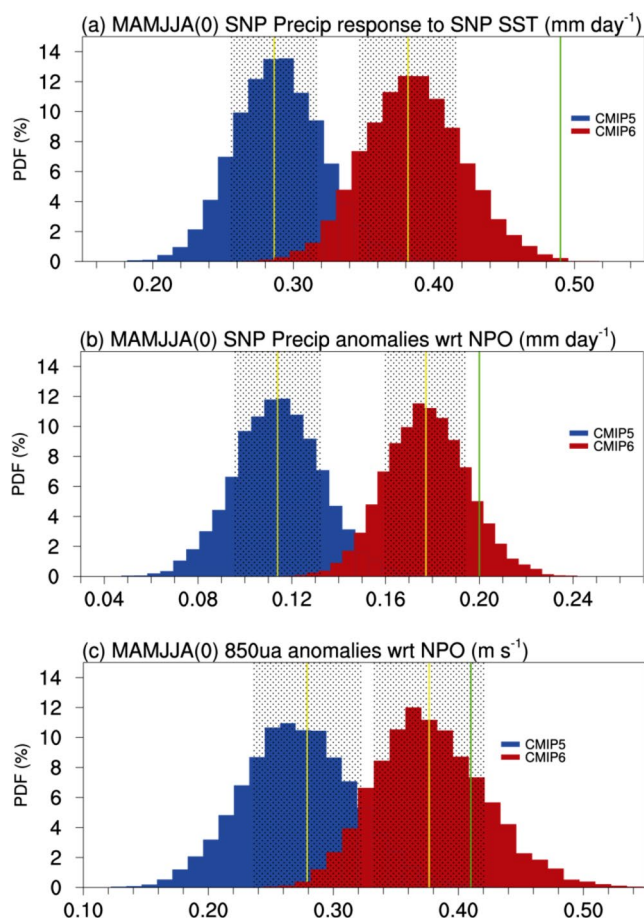


**Fig. 10** (a) Probability distributions of the 10,000 resampling with replacement of the bootstrap test for the MAMJJA(0) SNP precipitation anomalies regressed upon the MAMJJA(0) SNP SST index for the CMIP5 (blue) and CMIP6 (red). (b) and (c) as in (a), but for 10,000 resampling with replacement of the bootstrap test for the (b) MAMJJA(0) SNP precipitation anomalies and (c) MAMJJA(0) TWP 850-hPa zonal wind anomalies regressed upon the D(-1)JF(0) NPO index. Yellow lines in (a), (b) and (c) indicate the mean value of 10,000 resampling, with stippling regions indicating one s.d. of the 10,000 resampling. Green line indicates the observed result

respectively, both significant at the 95% confidence level. Overall, this result confirms previous findings (Okajima et al. 2003; Zhang et al. 2014; Zheng et al. 2023) that an equatorward shift of the spring-summer-mean ITCZ enhances the efficiency of the subtropical WES feedback and thus the impact of the winter NPO on the tropics.

We compared mean precipitation in MAMJJA(0) between observations and CMIP5/CMIP6 models (Fig. 12a-d). In the observations, mean ITCZ in spring and summer is located around 7.5°N in the northern Pacific (Fig. 12a). There is a strong positive precipitation bias over the subtropical southern Pacific, the well-known double ITCZ bias in current climate models (Fig. 12b-c). In addition, a strong positive precipitation bias is also found over the subtropical northern Pacific around 7.5°-20°N and 150°E-130°W (Fig. 12c).

This suggests a northward shift of the ITCZ in the CMIP5 compared to the observations. A comparison of the mean precipitation between CMIP6 and CMIP5 MMEs indicates a significant reduction in the positive precipitation bias over the subtropical Pacific (Fig. 12d). This suggests a southward shift of mean ITCZ location in the CMIP6 compared to the CMIP5 and indicates an improvement of the CMIP6 models in capturing the mean ITCZ structure (Tian and Dong 2020; Si et al. 2021). Therefore, a southward shift of mean ITCZ in spring and summer in CMIP6 compared to the CMIP5 may contribute to the enhancement of the subtropical WES feedback and explain the improved simulation of the impact of the winter NPO on the following winter ENSO (Okajima et al. 2003; Zhang et al. 2014; Zheng et al. 2023).

Studies indicated that the winter NPO could also impact the following winter ENSO via the trade wind charging mechanism (Anderson et al. 2013; Chakravorty et al. 2020) and the upper tropospheric mechanism (Zhao et al. 2023a, b). We have examined the winter NPO-related surface wind stress curl anomalies. Negative surface wind stress curl anomalies are seen in the subtropical North Pacific both in CMIP5 and CMIP6 (Fig. 13a-b), consistent with previous studies (Anderson et al. 2013; Chakravorty et al. 2020). The negative wind stress curl anomalies in the subtropical North Pacific contribute to subsurface oceanic temperature warming in the tropical central Pacific via modulating meridional heat transport, which play an important role in the following ENSO development. These suggest that both the CMIP5 and CMIP6 can well reproduce the trade wind charging mechanism. However, the differences in the surface wind stress curl anomalies in the subtropical North Pacific are weak between the CMIP5 and CMIP6 (Fig. 13c). This implies that the improved simulation of the winter NPO-ENSO relationship in CMIP6 is not likely due to the difference of the trade wind charging mechanism.

Recent studies also indicated that the winter NPO could impact the following winter ENSO via the upper tropospheric mechanism (Zhao et al. 2023a, b). Regarding the upper tropospheric mechanism, Zhao et al. (2023a) indicated that positive winter NPO could induce easterly wind anomalies in the upper tropospheric (e.g. 200 hPa) over the tropical Pacific via atmospheric wave propagation (Fig. 14a-b). These upper tropospheric easterly wind anomalies are simultaneously accompanied by lower-level westerly wind anomalies in the tropical western-central Pacific, which further influence the following winter ENSO development. However, the differences in the 200-hPa zonal wind anomalies over the tropical Pacific are weak (Fig. 14c). This suggests that improvement of the simulation of the influence of the winter NPO on the following winter ENSO is not attributed to the improved simulation of the upper tropospheric mechanism.

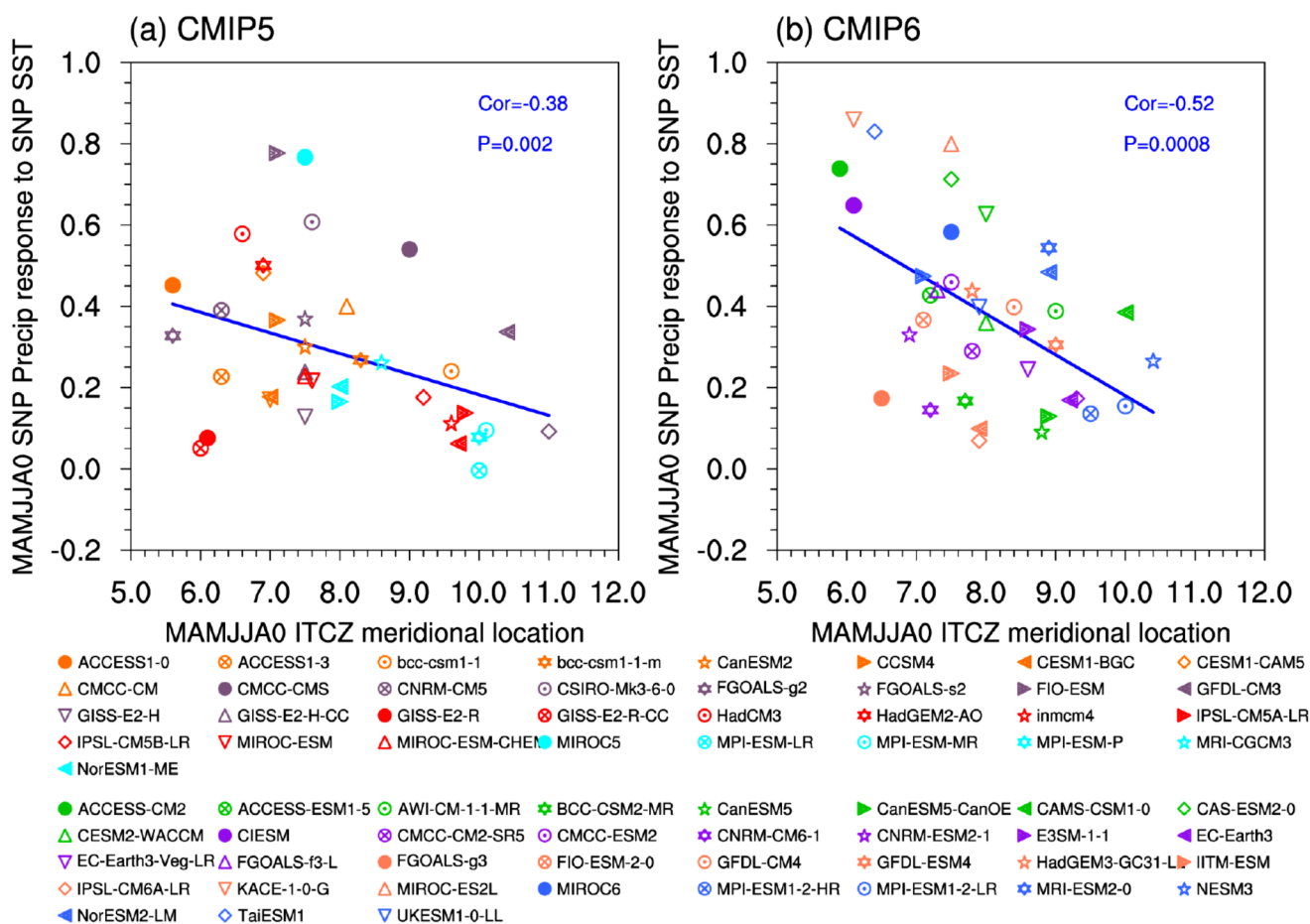


**Fig. 11** Scatter plot of the meridional location of the MAMJJA(0) ITCZ averaged over 180°-120°W (X-axis, degree latitude) versus MAMJJA(0) SNP precipitation anomalies regressed upon the MAM-

JJA(0) SNP SST anomalies (Y-axis, mm day<sup>-1</sup>) among the (a) 37 CMIP5 and (b) 39 CMIP6 models

### 5 Summary and discussions

The NPO is a prominent pattern of atmospheric variability over the North Pacific, and it plays a significant role in the occurrence and development of ENSO in the following winter. Most previous coupled climate models participating in CMIP5 tend to underestimate the relationship between winter NPO and the following winter ENSO. In particular, in most CMIP5 climate models, winter NPO-related surface winds and SST anomalies over the subtropical North Pacific are unable to extend equatorward to the tropical Pacific due to a weak WES feedback, and thus have a weak impact on the ENSO. This study revealed that the climate models in CMIP6 show an improvement in simulating the impact of winter NPO on ENSO. This improvement is related to the enhanced subtropical WES feedback and the associated enhanced precipitation and atmospheric anomalies response to subtropical North Pacific SST anomalies. Further analysis indicates that the enhanced WES feedback over the subtropical North Pacific is attributable to southward shift of

simulated mean ITCZ in CMIP6 compared to the CMIP5. The equatorward shift of the North Pacific ITCZ in CMIP6 is more favorable to the equatorward propagation of the SST and surface wind anomalies generated by the winter NPO, and thereby exerts a stronger influence on the subsequent winter ENSO.

The strength of the air-sea interaction could be influenced by the mean SST state (Chen et al. 2015b; Chen and Wu 2017). A higher mean SST state could favour a stronger air-sea interaction. To investigate the role of the mean SST state in the improved simulation of the relationship between the winter NPO and ENSO, we examined the difference in the mean SST state between the CMIP6 MME and the CMIP5 MME (Fig. 15). Figure 15 shows that the differences in the mean SST state between CMIP6 and CMIP5 are weak in most parts of the subtropical North Pacific and the tropical Pacific. This suggests that an improvement in the influence of the winter NPO on the subsequent winter ENSO in CMIP6 compared to CMIP5 is unlikely due to changes in the mean SST state.

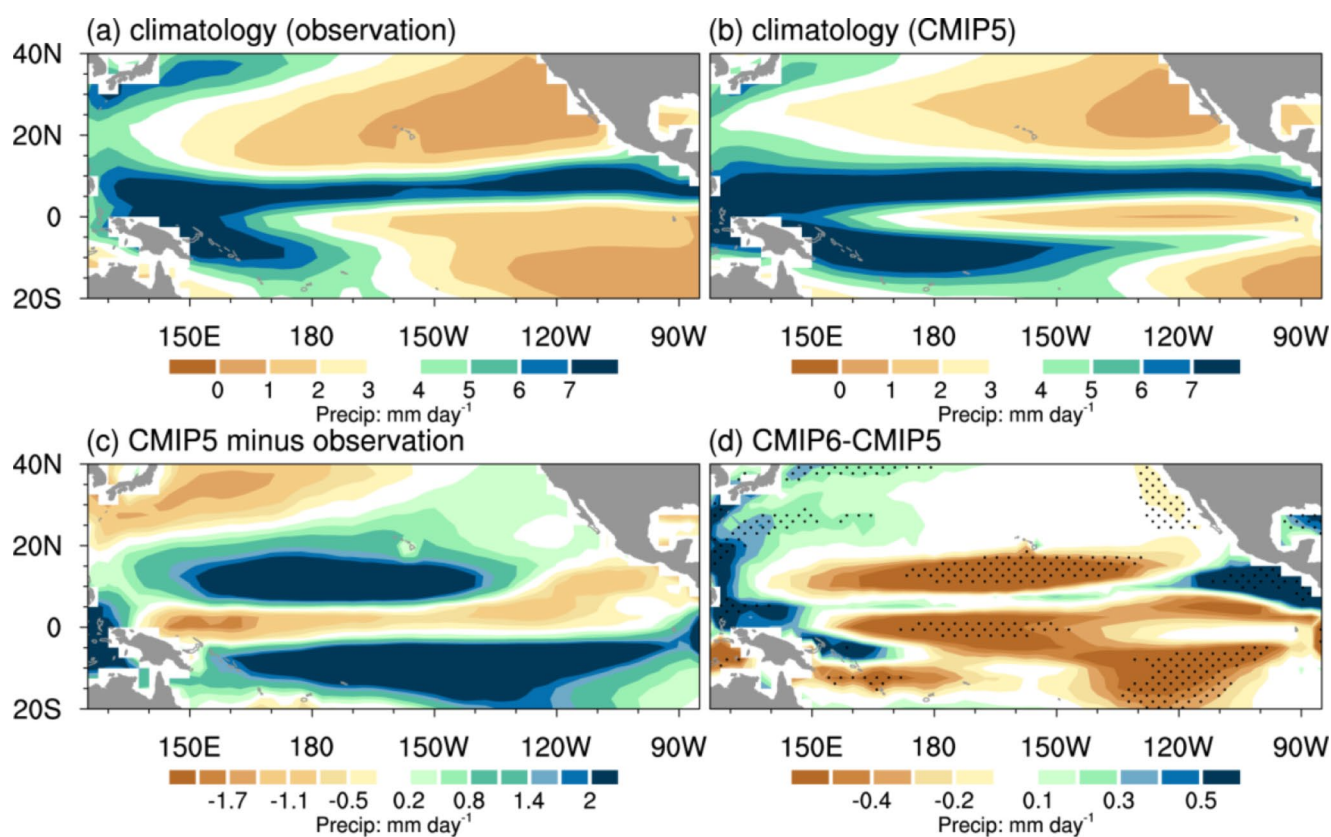


**Fig. 12** Climatology of MAMJJA(0) precipitation ( $\text{mm day}^{-1}$ ) in the (a) observations and (b) the MME of the 37 CMIP5 models. (c) is the difference in the climatology of MAMJJA(0) precipitation between CMIP5 MME and observations. (d) is the difference in the climatology

of MAMJJA(0) precipitation between CMIP6 MME and CMIP5 MME. Stippling region in (d) indicates the difference significant at the 5% level

Previous studies attributed the formation of the winter NPO-related low-level wind anomalies over the western equatorial Pacific mainly to the WES feedback over the subtropical North Pacific (Vimont et al. 2001; Alexander et al. 2010). Recent studies have shown that low-level westerly wind anomalies over the tropical western Pacific can also be modulated by other factors, such as the northern tropical Atlantic SST anomalies (Jia et al. 2021), the Aleutian low (Zheng et al. 2024), the Arctic sea ice (Chen et al. 2020b), the North Pacific meridional mode (Amaya 2019; Cheng et al. 2024b), and the South Pacific meridional mode (Zhang et al. 2014; Ding et al. 2015). The role of these factors in modulating the influence of the winter NPO on the subsequent winter ENSO in CMIP5 and CMIP6 models should be further investigated.

The monthly evolution of the standard deviation of the monthly Niño3.4 SST index is improved in CMIP6 compared to CMIP5 (Fig. 3). One may wonder whether this phenomenon is related to the improved simulation of the NPO influence on ENSO in CMIP6 or not. Figure 16a and c show the standard deviations of the raw SST anomalies for the CMIP5 MME and the CMIP6 MME, respectively. Large values of standard deviations are seen in the tropical

central eastern Pacific in both CMIP5 and CMIP6 models. The difference map shows that the standard deviations of the SST anomalies in the tropical central-eastern Pacific are much larger in CMIP6 than in CMIP5 (Fig. 16e). We then investigate whether the stronger amplitude of SST anomalies in the tropical central-eastern Pacific in CMIP6 is due to the improved simulation of the influence of the winter NPO on ENSO. To address this question, we have removed the signal associated with the D-1JF0 NPO index from the raw SST anomaly fields using a linear regression method. After linearly removing the effect of the winter NPO, the standard deviation of SST anomalies in DJF1 in the tropical central eastern Pacific is still significantly larger in CMIP6 than in CMIP5, although the amplitude of the difference decreases to some extent (Fig. 16f). This suggests that the stronger ENSO amplitude in CMIP6 may be only partly due to the improved simulation of the influence of the winter NPO on ENSO. It should be noted that ENSO variability is influenced by a number of factors, including tropical and extratropical forcings (Bjerknes 1969; Anderson et al. 2013; Chen et al. 2014; Amaya 2019). In addition to the NPO, other processes should also be crucial for the improved

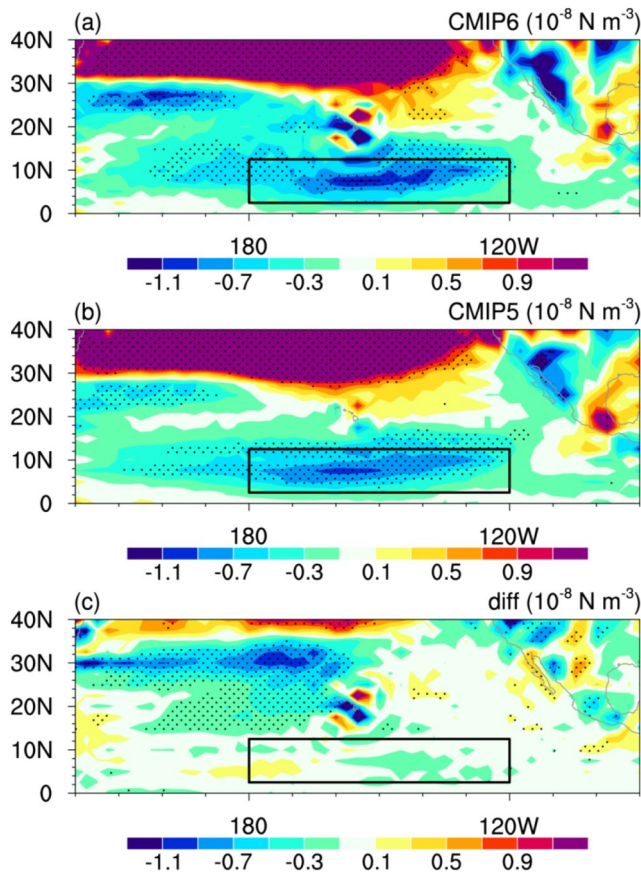


**Fig. 13** Surface wind stress curl anomalies ( $10^{-8} \text{ N m}^{-3}$ ) in D(-1)JF(0) regressed upon the D(-1)JF(0) NPO index over 1900–2003 for the CMIP6 MME (a), and CMIP5 MME (b), and the differences between CMIP6 and CMIP5 (c). Stippling regions in (a)–(b) indicate anomalies significant at the 95% confidence level. Stippling regions in (c) indicate the differences that are significantly different from zero at the 95% confidence level

simulation of ENSO variability in CMIP6, which should be further examined.

Previous studies suggest that ENSO can influence NPO (the Western Pacific pattern, WP) (Horel and Wallace 1981; Kodera 1998; Dai and Tan 2016; Aru et al. 2023a, b), and this influence is possibly by modulating a type of WP that is preceded by the Pacific/North American pattern (PNA) (Dai and Tan 2019). Therefore, there is a possibility that ENSO may influence the subsequent winter NPO (WP) through the seasonal footprinting mechanism. The ability of the CMIP5 and CMIP6 models to simulate the interaction between the ENSO and NPO could be further explored.

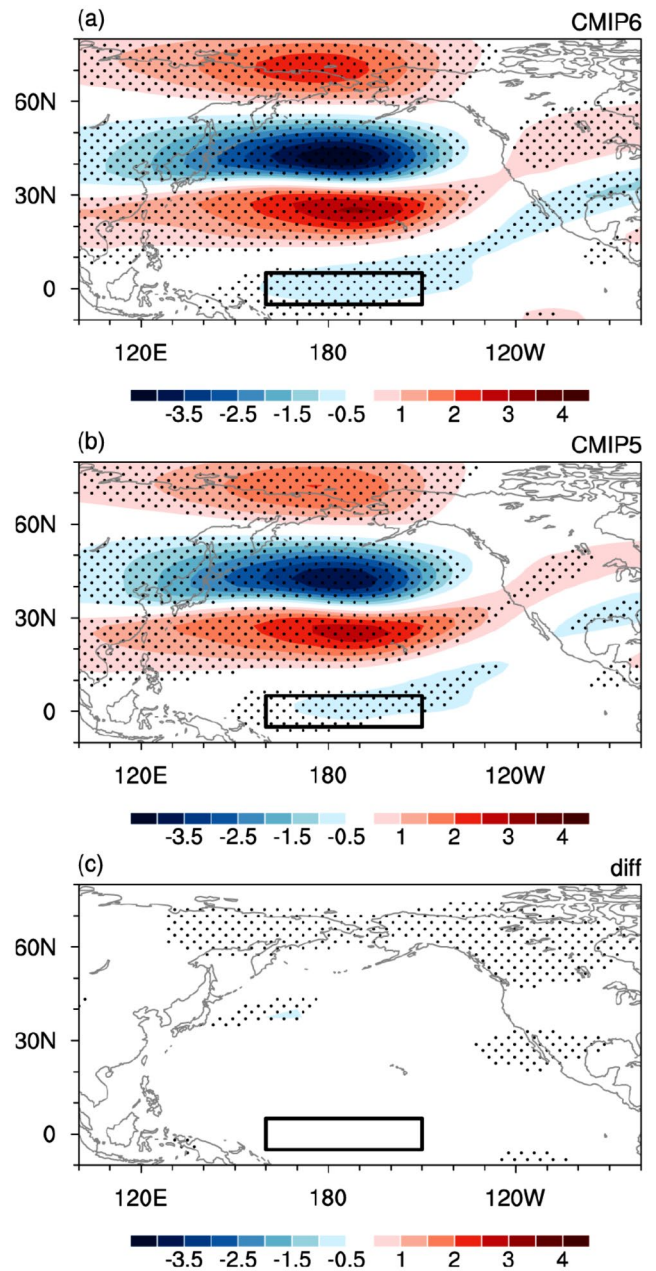


**Fig. 14** 200-hPa zonal wind anomalies ( $\text{m s}^{-1}$ ) in D(-1)JF(0) regressed upon the D(-1)JF(0) NPO index over 1900–2003 for the CMIP6 MME (a), and CMIP5 MME (b), and the differences between CMIP6 and CMIP5 (c). Stippling regions in (a)–(b) indicate anomalies significant at the 95% confidence level. Stippling regions in (c) indicate the differences that are significantly different from zero at the 95% confidence level

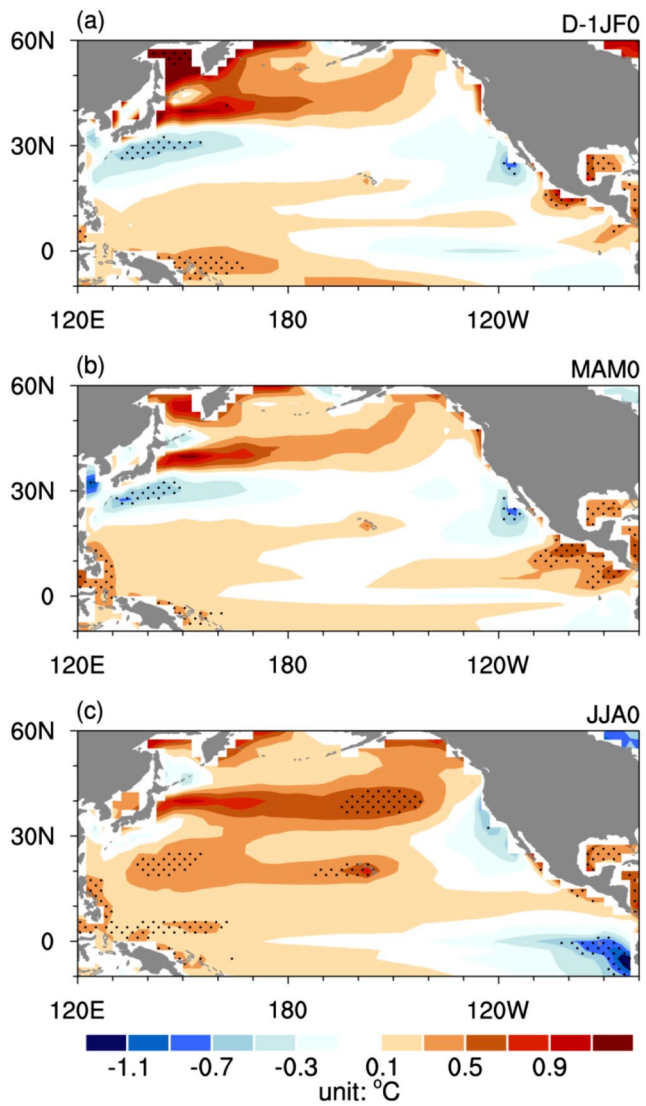


**Fig. 15** Difference in the climatology of SST between CMIP6 MME and CMIP5 MME in (a) D-1JF0, (b) MAM0 and (c) JJA0. Stippling regions in (a)-(c) indicates the difference significant at the 5% level



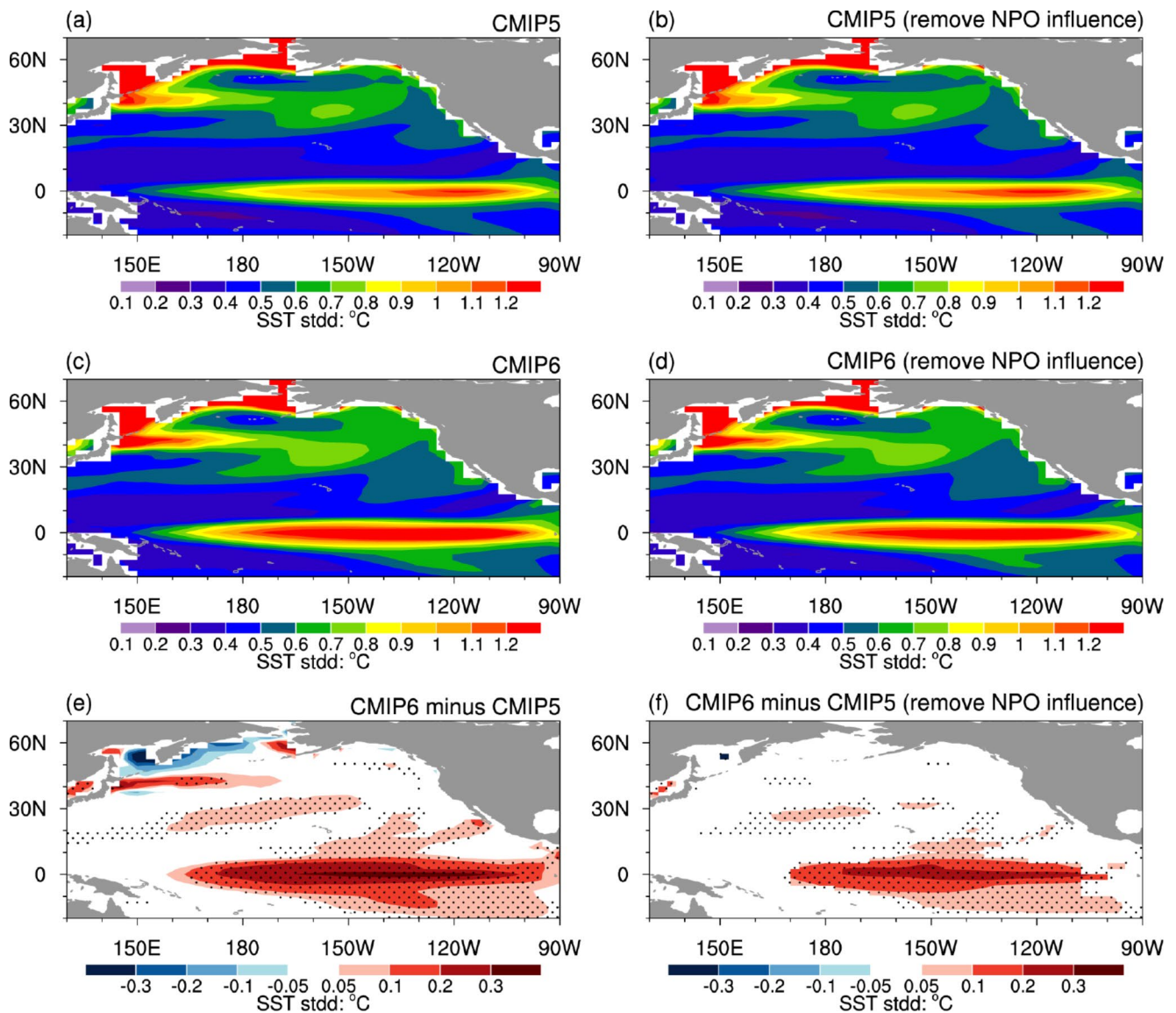


**Fig. 16** Standard deviation of SST anomalies in boreal winter for the (a) CMIP5 MME and (c) CMIP6 MME. (e) is the difference between (c) and (a). (b), (d) and (f) are the same as in (a), (c), (e), but winter

NPO index-related anomalies have been removed from the original SST fields. Stippling regions in (e)–(f) indicates the differences significant at the 5% level

**Authors' contributions** S.F.C. and W.C. designed the research, S.F.C. performed the analysis and wrote the manuscript. All authors commented and revised the manuscript.

**Code availability** All codes used in this study are available from the corresponding author.

**Funding** This work was supported by the National Natural Science Foundation of China (Grants 42175039, 42475042, 42230605 and 41975051), and the Key Laboratory of Meteorological Disaster, Ministry of Education (Nanjing University of Information Science & Technology) open project (KLME202201).

## Declarations

**Ethics approval and consent to participate** Not applicable.

**Consent for publication** Not applicable.

**Conflict of interest** The authors declare no potential conflicts of interest.

**Data availability** The NCEP-NCAR reanalysis data are derived from <https://psl.noaa.gov/data/gridded/data.ncep.reanalysis.html>. The ERSSTv5 data are available obtained from <https://www.ncdc.noaa.gov/data-access/marineocean-data/>. The GPCP data are derived from <https://psl.noaa.gov/data/gridded/data.gpcp.html>. The CMIP5 and CMIP6 data are derived from <https://esgf-node.llnl.gov/search/>. All figures were constructed with the NCAR Command Language (<http://www.ncl.ucar.edu/>).

## References

- Adler RF et al (2003) The version-2 global precipitation climatology project (GPCP) monthly precipitation analysis (1979–present). *J Hydrometeorol* 4:1147–1167
- Alexander MA, Blade I, Newman M, Lanzante JR, Lau NC, Scott JD (2002) The atmospheric bridge: the influence of ENSO teleconnections on air-sea interaction over the global oceans. *J Clim* 15:2205–2231
- Alexander MA, Vimont DJ, Chang P, Scott JD (2010) The impact of extratropical atmospheric variability on ENSO: testing the seasonal footprinting mechanism using coupled model experiments. *J Clim* 23:2885–2901
- Amaya DJ (2019) The Pacific Meridional Mode and ENSO: a review. *Curr Clim Change Rep* 5:296–307
- Anderson BT, Perez RC, Karspeck A (2013) Triggering of El Niño onset through trade wind-induced charging of the equatorial Pacific. *Geophys Res Lett* 40:1212–1216
- Aru HS, Chen W, Chen S (2021) Is there any improvement in Simulation of the Wintertime Western Pacific Teleconnection Pattern and Associated Climate anomalies in CMIP6 compared to CMIP5 models? *J Clim* 34:8841–8861
- Aru HS, Chen SF, Chen W (2022) Change in the variability in the Western Pacific pattern during boreal winter: roles of tropical Pacific sea surface temperature anomalies and North Pacific storm track activity. *Clim Dyn* 58:2451–2468
- Aru HS, Chen W, Chen SF, Garfinkel CI, Ma T, Dong Z, Hu P (2023a) Variation in the impact of ENSO on the western Pacific pattern influenced by ENSO amplitude in CMIP6 simulations. *J Geophys Res: Atmos* 128(22):e2022JD037905
- Aru HS, Chen W, Chen SF, An XD, Ma T, Cai QY (2023b) Asymmetrical modulation of the relationship between the western Pacific pattern and El Niño–Southern Oscillation by the Atlantic Multidecadal Oscillation in the boreal winter. *Geophys Res Lett* 50(14). <https://doi.org/10.1029/2023GL103356>
- Austin PC, Tu JV (2004) Bootstrap methods for developing predictive models. *Am Stat* 58:131–137
- Barnston AG, Tippett MK, L’Heureux ML, Li SH, DeWitt DG (2012) Skill of real-time seasonal ENSO model predictions during 2002–11 is our capability increasing? *Bull Amer Meteor Soc* 93:631–651
- Bjerknes J (1969) Atmospheric teleconnections from the equatorial Pacific. *Mon Wea Rev* 97:163–172
- Cai W et al (2020) Climate impacts of the El Niño–Southern Oscillation on South America. *Nat Rev Earth Environ* 1:215–231
- Cai QY, Chen W, Chen SF, Xie SP, Piao JL, Ma TJ, Lan XQ (2024) Recent pronounced warming on the Mongolian Plateau boosted by internal climate variability. *Nat Geosci* 17:181–188
- Chakravorty S, Perez RC, Anderson BT, Giese BS, Larson SM, Pivotti V (2020) Testing the Trade wind charging mechanism and its influence on ENSO variability. *J Clim* 33:7391–7411
- Chang P, Zhang L, Saravanan R, Vimont DJ, Chiang JCH, Ji L, Seidel H, Tippett MK (2007) Pacific Meridional mode and El Niño–Southern Oscillation. *Geophys Res Lett* 34:L16608
- Chen SF, Wu R (2017) Interdecadal changes in the relationship between interannual variations of spring north Atlantic SST and Eurasian surface air temperature. *J Clim* 30:3771–3787
- Chen SF, Wu R (2018) Impacts of winter NPO on subsequent winter ENSO: sensitivity to the definition of NPO index. *Clim Dyn* 50:375–389
- Chen SF, Yu B (2020) The seasonal footprinting mechanism in large ensemble simulations of the second generation Canadian Earth System Model: uncertainty due to internal climate variability. *Clim Dyn* 55:2523–2541
- Chen W, Feng J, Wu R (2013) Roles of ENSO and PDO in the link of the east Asian winter monsoon to the following summer monsoon. *J Clim* 26(2):622–635
- Chen SF, Yu B, Chen W (2014) An analysis on the physical process of the influence of AO on ENSO. *Clim Dyn* 42:973–989
- Chen SF, Wu R, Chen W (2015b) The changing relationship between interannual variations of the North Atlantic Oscillation and northern tropical Atlantic SST. *J Clim* 28:485–504
- Chen DK, Lian T, Fu C, Cane M, Tang Y, Murtugudde R, Song X, Wu Q, Zhou L (2015a) Strong influence of westerly wind bursts on El Niño diversity. *Nat Geosci* 8:339–345
- Chen SF, Song LY, Chen W (2019) Interdecadal Modulation of AMO on the Winter North Pacific Oscillation-following Winter ENSO Relationship. *Adv Atmos Sci* 36:1393–1403
- Chen SF, Chen W, Wu R, Yu B, Graf HF (2020a) Potential impact of preceding Aleutian Low variation on the El Niño–Southern Oscillation during the following winter. *J Clim* 33:3061–3077
- Chen SF, Wu R, Chen W, Yu B (2020b) Influence of winter Arctic Sea ice concentration change on the El Niño–Southern Oscillation in the following winter. *Clim Dyn* 54(1):741–757
- Chen SF, Yu B, Wu R, Chen W, Song L (2021) The dominant North Pacific atmospheric circulation patterns and their relations to Pacific SSTs: historical simulations and future projections in the IPCC AR6 models. *Clim Dyn* 56:701–725
- Chen SF, Chen W, Yu B, Wu R, Graf HF, Chen L (2023a) Enhanced impact of the Aleutian Low on increasing the Central Pacific ENSO in recent decades. *npj Clim Atmos Sci* 6:29
- Chen SF, Chen W, Yu B, Wu L, Chen L, Li ZB, Aru HS, Huangfu JL (2023b) Impact of the winter Arctic Sea ice anomaly on the following summer tropical cyclone genesis frequency over the western North Pacific. *Clim Dyn* 61:3971–3988
- Chen SF, Chen W, Xie SP, Yu B, Wu R, Wang ZB, Lan XQ, Graf HF (2024a) Strengthened impact of boreal winter North Pacific Oscillation on ENSO development in warming climate. *npj Clim Atmos Sci* 7:69
- Chen SF, Chen W, Wu R, Yu B, Ying J (2024b) Joint impacts of winter North Pacific Oscillation and early spring Aleutian Low intensity on the following winter ENSO. *Clim Dyn* 62(1):257–276
- Cheng X, Chen SF, Chen W, Hu P (2023) Observed impact of the Arctic Oscillation in boreal spring on the Indian Ocean Dipole in the following autumn and possible physical processes. *Clim Dyn* 61:883–902
- Cheng X, Chen SF, Chen W, Hu P, Du ZC, Lan XQ, Zheng YQ (2024b) How does the North Pacific Meridional Mode affect the Indian Ocean Dipole? *Clim Dynamics* 62:3123–3142
- Cheng X, Chen SF, Chen W, Wu R, Yang RW, Hu P, Chen L, Aru HS (2024a) Selective influence of the Arctic Oscillation on the Indian Ocean Dipole and El Niño–Southern Oscillation. *Clim Dyn* 62:3783–3798
- Dai Y, Tan B (2016) The western Pacific pattern precursor of major stratospheric sudden warmings and the ENSO modulation. *Environ Res Lett* 11:124032
- Dai Y, Tan B (2019) Two types of the western Pacific pattern, their climate impacts, and the ENSO modulation. *J Clim* 32:823–841
- Ding RQ, Li JP, Tseng YH (2015) The impact of South Pacific extratropical forcing on ENSO and comparisons with the North Pacific. *Clim Dyn* 44:2017–2034
- Ding RQ et al (2022) Multi-year El Niño events tied to the North Pacific Oscillation. *Nat Commun* 13:3871
- Eyring V, Bony S, Meehl GA, Senior CA, Stevens B, Stouffer RJ, Taylor KE (2016) Overview of the coupled model Intercomparison Project Phase 6 (CMIP6) experimental design and organization. *Geosci Model Dev* 9:1937–1958
- Ham YG, Kug JS, Park JY, Jin FF (2013) Sea surface temperature in the north tropical Atlantic as a trigger for El Niño/Southern Oscillation events. *Nat Geosci* 6:112–116

- Horel JD, Wallace JM (1981) Planetary-scale atmospheric phenomena associated with the Southern Oscillation. *Mon Wea Rev* 109:813–829
- Huang B et al (2017) Extended reconstructed Sea Surface temperature version 5 (ERSSTv5), upgrades, validations, and intercomparisons. *J Clim* 30:8179–8205
- Jia F et al (2021) Enhanced North Pacific impact on El Niño/Southern Oscillation under greenhouse warming. *Nat Clim Change* 11:840–849
- Kalnay E et al (1996) The NCEP/NCAR 40-year reanalysis project. *Bull Amer Meteor Soc* 77(3):437–472
- Kodera K (1998) Consideration of the origin of the different midlatitude atmospheric responses among El Niño events. *J Meteor Soc Japan* 76:347–361
- Lee J et al (2019) Quantifying the agreement between observed and simulated extratropical modes of interannual variability. *Clim Dyn* 52:4057–4089
- Linkin ME, Nigam S (2008) The North Pacific Oscillation–West Pacific teleconnection pattern: mature-phase structure and winter impacts. *J Clim* 21:1979–1997
- Luo JJ, Masson S, Behera S, Yamagata T (2008) Extended ENSO predictions using a fully coupled ocean-atmosphere model. *J Clim* 21:84–93
- McPhaden MJ, Zebiak SE, Glantz MH (2006) ENSO as an integrating concept in Earth science. *Science* 314:1740–1745
- Min Q, Su J, Zhang R, Rong X (2017) Impact of the South and North Pacific meridional modes on the El Niño–Southern Oscillation: observational analysis and comparison. *J Clim* 30:1705–1720
- Nakamura T, Tachibana Y, Honda M, Yamane S (2006) Influence of the Northern Hemisphere annular mode on ENSO by modulating westerly wind bursts. *Geophys Res Lett* 33:L07709
- Neelin JD et al (1998) ENSO theory. *J Geophys Res* 103:14261–14290
- Okajima H, Xie SP, Numaguti A (2003) Interhemispheric coherence of tropical climate variability: effect of climatological ITCZ. *J Meteor Soc Japan* 81:1371–1386
- Park JH et al (2021) Role of the climatological intertropical convergence zone in the seasonal footprinting mechanism of the El Niño–Southern Oscillation. *J Clim* 34:5243–5256
- Ren HL, Zheng F, Luo JJ, Wang R, Liu M, Zhang W, Zhou T, Zhou G (2020) A review of research on tropical air-sea interaction, ENSO dynamics, and ENSO prediction in China. *Acta Meteorologica Sinica* 78:351–369
- Rogers JC (1981) The North Pacific Oscillation. *J Climatol* 1:39–57
- Si W, Liu H, Zhang X, Zhang M (2021) Double intertropical convergence zones in coupled ocean-atmosphere models: progress in CMIP6. *Geophys Res Lett* 48:e2021GL094779
- Song LY, Chen SF, Chen W, Duan WS, Li Y (2021) Interdecadal change in the relationship between boreal winter North Pacific Oscillation and Eastern Australian rainfall in the following autumn. *Clim Dyn* 57:3265–3283
- Tang YM, Zhang RH, Liu T, Duan W, Yang D, Zheng F, Ren HL, Lian T, Gao C, Chen DK, Mu M (2018) Progress in ENSO prediction and predictability study. *Natl Sci Rev* 5(6):826–839
- Taylor KE, Stouffer RJ, Meehl GA (2012) An overview of CMIP5 and the experiment design. *Bull Amer Meteor Soc* 93(4):485–498
- Tian B, Dong X (2020) The Double-ITCZ Bias in CMIP3, CMIP5, and CMIP6 models based on Annual Mean Precipitation. *Geophys Res Lett* 47(8):e2020GL087232
- Vimont DJ (2010) Transient growth of thermodynamically coupled variations in the tropics under an equatorially symmetric mean. *J Clim* 23:5771–5789
- Vimont DJ, Battisti DS, Hirst AC (2001) Footprinting: a seasonal connection between the tropics and mid-latitudes. *Geophys Res Lett* 28:3923–3926
- Vimont DJ, Wallace JM, Battisti DS (2003) The seasonal footprinting mechanism in the Pacific: implications for ENSO. *J Clim* 16:2668–2675
- Vimont D, Alexander M, Fontaine A (2008) Mid-latitude excitation of tropical variability in the Pacific: the role of thermodynamic coupling and seasonality. *J Clim* 22:518–534
- Walker GT, Bliss WE (1932) World weather V. *Memories of the royal meteorological. Society* 44:53–84
- Wang C (2019) Three-ocean interactions and climate variability: a review and perspective. *Clim Dyn* 53:18
- Wang B, Wu R, Fu X (2000) Pacific–East Asian teleconnection: how does ENSO affect east Asian. *Climate? J Clim* 13:1517–1536
- Wang X, Wang C, Zhou W, Wang D, Song J (2011) Teleconnected influence of North Atlantic sea surface temperature on the El Niño onset. *Clim Dyn* 37:663–676
- Wang X, Chen M, Wang C, Yeh SW, Tan W (2019) Evaluation of performance of CMIP5 models in simulating the North Pacific Oscillation and El Niño Modoki. *Clim Dyn* 52:1383–1394
- Webster PJ, Magana VO, Palmer TN, Shukla J, Tomas RA, Yanai M, Yasunari T (1998) Monsoons: processes, predictability, and the prospects for prediction. *J Geophys Res Atmos* 103:14451–14510
- Xiang B, Wang B, Yu W, Xu S (2013) How can anomalous western north Pacific subtropical high intensify in late summer? *Geophys Res Lett* 40:2349–2354
- Xie SP, Philander SGH (1994) A coupled ocean-atmosphere model of relevance to the ITCZ in the eastern Pacific. *Tellus Ser A-Dynamic Meteor Oceanogr* 46:340–350
- Xie SP et al (2009) Indian ocean capacitor effect on Indo-Western Pacific climate during the summer following El Niño. *J Clim* 22:730–747
- Yeh SW, Wang X, Wang C, Dewitte B (2015) On the relationship between the North Pacific climate variability and the Central Pacific El Niño. *J Clim* 28:663–677
- Yeh SW et al (2018) ENSO atmospheric teleconnections and their response to greenhouse gas forcing. *Rev Geophys* 56:185–206
- Yu JY, Kim ST (2011) Relationships between extratropical sea level pressure variations and the Central-Pacific and Eastern-Pacific types of ENSO. *J Clim* 24:708–720
- Zhang H, Deser C, Clement A, Tomas R (2014) Equatorial signatures of the Pacific Meridional modes: dependence on mean climate state. *Geophys Res Lett* 41:568–574
- Zhang RH, Min QY, Su JZ (2017) Impact of El Niño on atmospheric circulations over East Asia and rainfall in China: role of the anomalous western North Pacific anticyclone. *Sci China-Earth Sci* 60:1124–1132
- Zhang WJ, Wang Z, Stuecker MF, Turner AG, Jin FF, Geng X (2019) Impact of ENSO longitudinal position on teleconnections to the NAO. *Clim Dyn* 52:257–274
- Zhao W, Chen SF, Zhang H, Wang J, Chen W, Wu R, Xing W, Wang Z, Hu P, Piao J, Ma T (2022) Distinct impacts of ENSO on haze pollution in Beijing–Tianjin–Hebei region between early and late winters. *J Clim* 35:687–704
- Zhao J, Sung MK, Park JH, Luo JJ, Kug JS (2023a) Part I observational study on a new mechanism for North Pacific Oscillation influencing the tropics. *npj Clim Atmos Sci* 6(1):15
- Zhao J, Sung MK, Park JH, Luo JJ, Kug JS (2023b) Part II model support on a new mechanism for North Pacific Oscillation influence on ENSO. *npj Clim Atmos Sci* 6(1):16
- Zheng YQ, Chen W, Chen SF (2021) Intermodel spread in the impact of the springtime Pacific Meridional Mode on following-winter ENSO tied to simulation of the ITCZ in CMIP5/CMIP6. *Geophys Res Lett* 48: e2021GL093945
- Zheng YQ, Chen SF, Chen W, Yu B (2023) A continuing increase of the impact of the spring North Pacific Meridional Mode on the following winter El Niño and Southern Oscillation. *J Clim* 36(2):585–602

Zheng YQ, Chen SF, Chen W, Wu R, Wang ZB, Yu B, Hu P, Piao JL (2024) The role of the Aleutian Low in the relationship between spring Pacific Meridional Mode and following ENSO. *J Clim* 37(11):3249–3268

**Publisher's note** Springer Nature remains neutral with regard to jurisdictional claims in published maps and institutional affiliations.

Springer Nature or its licensor (e.g. a society or other partner) holds exclusive rights to this article under a publishing agreement with the author(s) or other rightsholder(s); author self-archiving of the accepted manuscript version of this article is solely governed by the terms of such publishing agreement and applicable law.